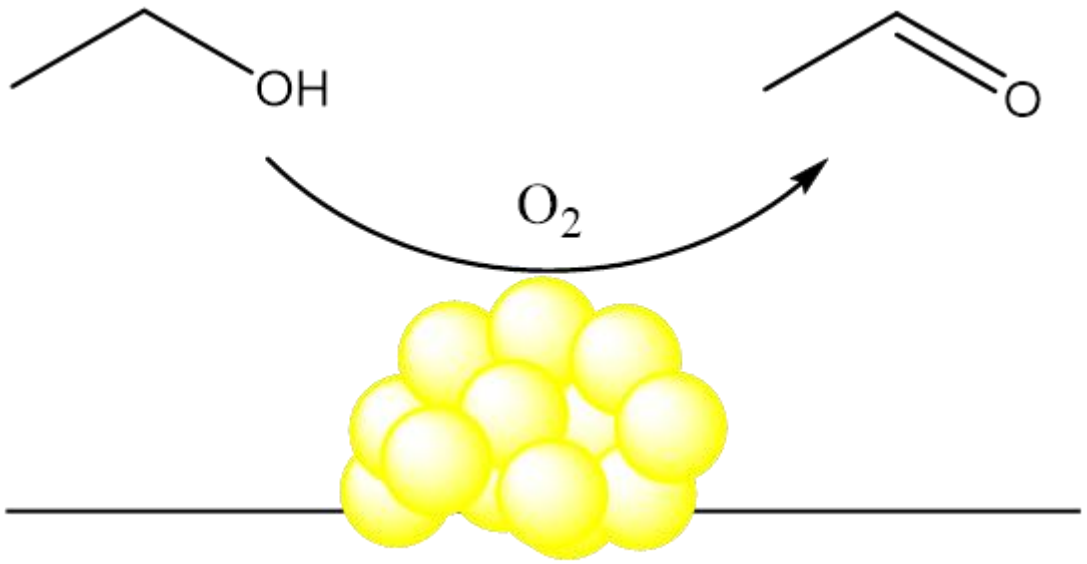

MASTER THESIS
NANOMATERIALS SCIENCE

Atomically Precise Gold Containing Clusters for Selective Ethanol Oxidation

A study of stability and activity of atomically precise gold containing clusters supported on SiO_2 and CeO_2 for selective aerobic oxidation of ethanol in gas phase.

Jorrit M. van Hoof (5741645)
j.m.hoof@students.uu.nl
Inorganic Chemistry and Catalysis, University Utrecht

Daily supervisor: dr. B. Donoeva
Second examiner: prof. dr. P.E. de Jongh

Universiteit Utrecht

Layman's abstract

A catalyst is a substance that can be used to reduce the amount of energy required for a certain chemical reaction, often speeding up the reaction. A perfect catalyst is not altered hereafter and can undergo unlimited chemical reactions without deactivation. Using catalysts can also often result in more specificity towards a certain desired product, reducing the number of unwanted by-products as waste. One such catalyst is gold (Au), but only if the gold particle sizes are decreased to a certain nanosize in diameter (d < 100 nm). Ultra-small Au particles composed of only a few Au atoms (d < 2 nm), called nanoclusters, can catalytically dissociate molecular oxygen (O_2) which can be used in chemical oxidation reactions from a green viewpoint. These nanoclusters can be prepared in many ways. One way is to chemical synthesis. This way, clusters are synthesised with high precision and are composed of a few Au atoms as a core protected by ligands around it. These protective ligands must first often be removed to activate the catalyst. The nanoclusters tend to aggregate to form larger particles fairly easily upon removing the protective ligands, called sintering. To prevent sintering, the clusters must be deposited onto a solid supporting material that can stabilise them (like ceria, CeO_2). This way, the characteristics of the Au clusters can be further investigated as it is yet unknown how catalytic activity evolves in this small cluster size regime. In this research, CeO_2 rods and cubes are synthesised that prevent sintering of the nanoclusters after heat treatment whereas CeO_2 polyhedra do not. Various clusters are deposited on CeO_2 rods to test their catalytic activity in ethanol oxidation. Single atom removal from the Au core (Au_9 → Au_8) resulted in a decrease in catalytic activity, whereas the use of a bimetallic cluster (Au_6Pd) did not show a significantly higher activity. Furthermore, larger Au nanoparticles did show a substantial higher activity than all used Au clusters. Hereafter, Au_9 clusters are deposited on another solid material (silica, SiO_2) that is less likely to stabilise the clusters. This sample is treated with a solution containing boron trichloride (BCl_3) to chemically remove the protective ligands around the Au core of Au_9 clusters without changing the cluster size. Even though the ligands were chemically removed this way, most of the clusters were dislodged from the SiO_2 surface and the ones remaining grew to form larger particles. This means that the chemical removal of ligands using BCl_3 was an unsuitable method to investigate the activity of Au clusters.

Abstract

Conventional nanocatalysts have a nonuniform particle size distribution, while catalytic activity of nanoparticles is size dependent. This is also the case for gold as the intrinsic chemical properties of very small gold particles (called Au clusters) are strongly dependent on its size and composition. It is, however, unknown how the catalytic activity evolves in this nanosized regime. Sintering of these clusters could be prevented by using a suitable support material and without calcination at high temperatures. In this research, the activity and stability of various Au nanoclusters are investigated. In order to do this, CeO_2 rods, cubes and polyhedra are synthesised as support material exhibiting ({110} and {111}), {100} and ({100} and {111}) exposed surface planes respectively because these tend to have different stabilising properties. After deposition of Au_9 clusters on each CeO_2 material and heat treatment, the rods and cubes showed least nanoparticle formation. Hereafter, Au_8, Au_6Pd are deposited and Au nanoparticles were grown on CeO_2 rods because this material seemed to prevent sintering. These catalysts were subsequently tested in the gas phase oxidation of ethanol using O_2. The Au nanoparticles showed the highest activity, but its higher selectivity towards CO_2 also resulted in possible polycarbonate species bound to the CeO_2 surface which lead to deactivation. Furthermore, a decrease of cluster size by only one atom (Au_9 → Au_8) resulted in a decrease in oxidation activity, while a bimetallic cluster (Au_6Pd) did not show a much higher activity contrary to previous believes. Next to this, Au_9 clusters deposited on SiO_2 are treated with BCl_3 to chemically remove its protecting ligands. This resulted in growth of the Au nanoparticle size and Au leaching. This makes BCl_3 treatment an unsuitable method for chemical ligand removal to investigate the properties of various Au clusters on inert supports.

Contents

Layman's abstract 1
Abstract 2
Contents 3
1. Introduction 4
1.1 Gold nanoclusters 4
1.2 Gold clusters synthesis 5
1.3 Catalysis with gold clusters 5
1.4 CeO_2 support material 7
1.2 Goal of research 10
1.3 Approach 10
2. Theory 11
2.3 Transmission Electron Microscopy 12
2. Experimental section 13
2.1 Catalyst characterisation 13
2.2 CeO_2 support synthesis 13
2.3 Gold nanoclusters synthesis 13
2.3.1 $AuPPh_3NO_3$ 13
2.3.3 $AuPPh_3Cl$ 13
2.3.4 $[Au_9(PPh_3)_8](NO_3)_3$ 14
2.3.5 $[Au_8(PPh_3)_8](NO_3)_2$ 14
2.3.6 $[Au_8Pd(PPh_3)_8]Cl_2$ 14
2.3.7 $[Au_6Pd(PPh_3)_7](NO_3)_2$ 14
2.4 Cluster deposition 15
2.5 Au_n-CeO_2 15
2.6 Chemical ligand removal 15
2.7 Catalytic experiments 15
3. Results and Discussion 17
3.1 CeO_2 crystals characterisation 17
3.2 Heat treatments of Au_9-CeO_2 20
3.3 Catalytic oxidation of ethanol 22
3.4 Chemical ligand removal from Au_9-SiO_2 27
4. Conclusion 29
5. Outlook 29
6. Acknowledgements 30
7. References 31
8. Supplementary information 36

1. Introduction

1.1 Gold nanoclusters

Since gold (Au) is one of the least reactive metals, it has been regarded as poorly active in heterogeneous catalysis. However, most of our knowledge back in the day has come from the chemistry of smooth Au surfaces or of relatively large Au particles with diameters above 10 nm. In the 1980s, Haruta and co-workers found that its chemistry dramatically changes when Au is deposited as ultra-fine particles on various oxides leading to high activities in CO oxidation.[1,2] Their results for H_2 and CO oxidation are shown in Figure 1. Particles below 10 nm show a much lower temperature for 50% oxidation ($T_{½}$) which is correlated to a higher activity. These particles have already been used for commercial applications in offensive odour removal and gas sensors.[3] Recent experiments have shown that gold clusters (<2 nm in diameter) supported on inert supports such as SiO_2 could catalyse styrene epoxidation in the liquid phase and propylene epoxidation in gas phase with molecular oxygen as oxidant, while gold nanoparticles (>2.0 nm) were inactive.[4–6] This indicated that gold clusters themselves can efficiently activate molecular oxygen. This allows the selective oxidation of hydrocarbons using oxygen from air which later increased in interest from the viewpoint of green chemistry.

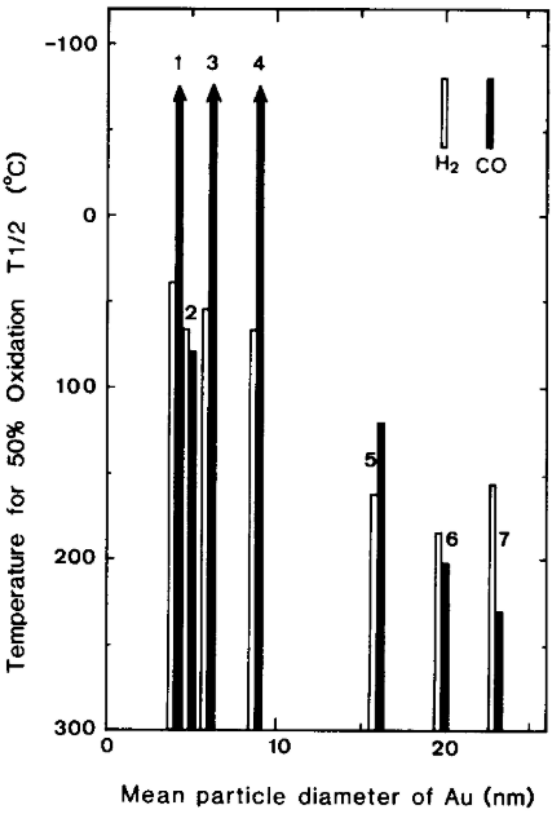

Figure 1. Catalytic activities for H_2 and CO oxidation as a function of mean particle diameter of Au. Adapted from Haruta *et al*.[1]

The chemical properties of metal clusters can be drastically altered by varying the number of atoms it consists out of (i.e. cluster size).[7,8] This has been shown in the case of Au nanoclusters. Their catalytic activity increases with decreasing the size to a certain point in several cases.[9,10] For example, Tsunoyama and colleagues[11] have synthesised Au clusters and supported them on hydroxyapatite (HAP). Au_{39} showed an optimum in total selectivity and turn-over frequencies in oxidation of cyclohexane towards KA oil (cyclohexanol and cyclohexanone). These metal cluster's chemical properties differ greatly from those of the corresponding bulk metal and nanoparticles, because of their quantized electronic structures and unique geometrical structures. Even changing the cluster size by one atom may change its catalytic activity and selectivity.[12] Another interesting result is the presence a distinct "odd-even" alteration, that is, cationic and anionic clusters with an odd number of atoms have low reactivity, since they have an even valence electron count.[13,14] This means that odd numbered clusters have and unpaired valence electron which can be donated more easily to a substrate molecule (like O_2) compared to paired valence electron in even numbered clusters.[15] This odd-even oscillation is also shown by Nijamudheen *et al.*[16] and their results are shown in Figure 2. An oscillation is observed in both HOMO-LUMO gaps and adsorption wavelengths (λ_{max}). Also, an overall red shift is observed with increasing size of the Au clusters (Figure 2b)

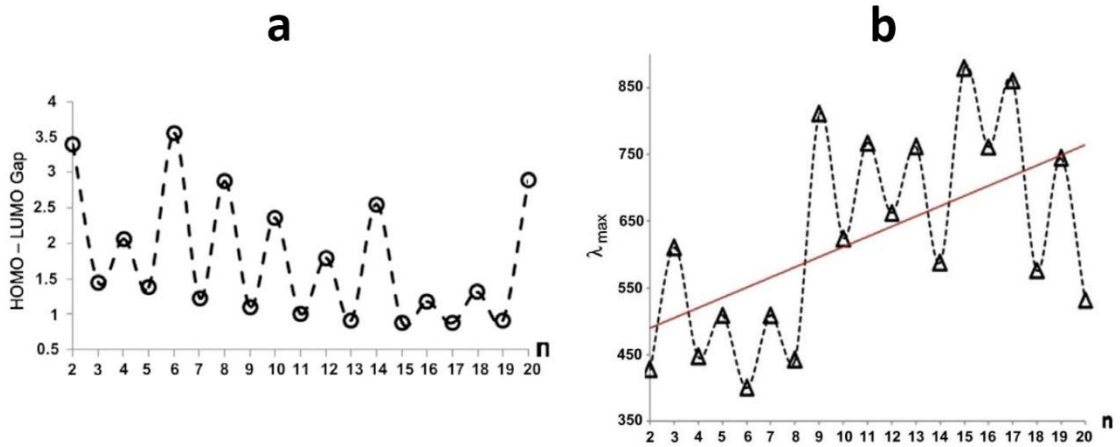

Figure 2. HOMO-LUMO gaps in eV (a) and profile for the variation of absorption wavelength λ_{max} in nm (b) with respect to the size of the clusters (*n*). Adapted from A. Nijamudheen *et al.*[16]

1.2 Gold clusters synthesis

There are numerous ways to synthesise Au clusters, for example; physical vapor deposition, electrical reduction and solid grinding.[17] Another way to synthesise these clusters is by chemical reduction. This method makes use of a synthesis system composed of the gold precursor, solvent, protecting ligands, and reducing agent. Changing any of these chemicals or even a ratio between them can result in a whole other cluster which makes this a very sensitive synthesis method.[18] The protecting ligands are bound with the surface gold atom to prevent the growth of nuclei towards nanoparticles, and thereby leading to the formation of small gold clusters in a narrow size distribution. In the case of cluster synthesis a strong reducing agent (such as $NaBH_4$) is often used to prevent the slow formation of larger nanoparticles when a weak reducing agent is used.

This way, Au_n clusters have been successfully synthesised, mostly stabilised by either thiolates[11,18–20] or phosphine[18,21,22] ligands in the past. Unlike thiolate-stabilised Au clusters, phosphine stabilised clusters can be synthesised in both low atomic range ($n < 15$) and higher atomicity range ($n = 20, 25, 39, 54, 101$, etc.) and hence are suitable precursors for the synthesis of both sub- and supra-nm atomically precise supported Au clusters.[23] Only a few of them could be crystallized and examined with single-crystal X-ray diffraction, which enables a precise determination of the structure of the cluster core with ligand shell.

1.3 Catalysis with gold clusters

Gold clusters have been used to catalyse some typical reactions including selective hydrogenation of unsaturated aldehydes and ketones; selective oxidation of alkanes, alkenes and alcohols; CO oxidation; and organic synthesis. Especially the selective oxidation is of high importance to the chemical industry as the resulting products such as aldehydes, ketones, epoxides and acids are widely used to produce polymers, surfactants, detergents, cosmetics and so on.[24,25] Gold clusters have displayed the unique capability in catalysing this type of reactions.

In 1998, Pratis *et al.*[26] found out that gold could efficiently catalyse the selective oxidation of diols with molecular oxygen as an oxidant in the liquid phase. Later, gold nanoparticles and clusters were widely investigated in the selective oxidation of various alcohols. It was found out that once supported the clusters show a higher catalytic activity after removal of protecting ligands.[27] This removal could be done by calcination, which oxidizes the ligands at high temperatures often leading to Au particle growth.[28] Recent (unpublished) research in our group has shown that the phosphine ligands around the cluster's Au core can be easily removed after deposition on a Lewis acidic support by heating the supported

clusters at 120 °C for 4h. This relative low temperature treatment resulted in the phosphine ligands poisoning the Lewis acidic sites of the support while keeping the cluster atomicity intact shown in Figure 3.

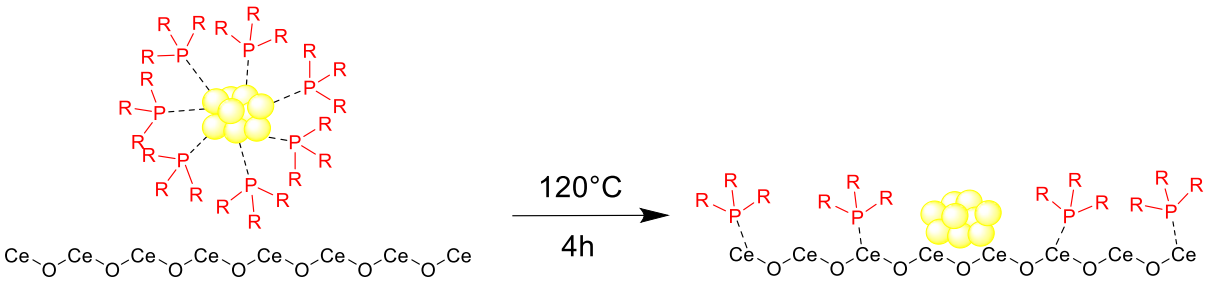

Figure 3. Schematic display of the removal of protective ligands around a Au_9 cluster on CeO_2. Note that some ligands are omitted on the right for clarity.

Clusters have also been deposited on numerous other solid supports or stabilised by polymers like PVP (poly(N-vinyl-2-pyrrolidone)). Tsynoyama *et al.*[29,30] have synthesised clusters of varying sizes (1.3 nm to 9.5 nm) in the presence of PVP as the stabiliser and tested them in the aerobic oxidation of p-hydroxybenzyl alcohol. They found a rapid increase in turnover frequencies (TOF) based on surface gold atoms with decreasing size of clusters. Adnan *et al.*[28] have deposited Au_8 and Au_9 on TiO_2 for aerobic oxidation of benzyl alcohol. They found that after deposition, the clusters tend to be inactive, even after calcination under oxygen. However, if H_2 is added during calcination, the clusters (which have become larger particles after calcination) showed an increase in conversion with decreasing size. They suggested that the calcination with H_2 changes the nature of NO_3^- species resulting in them not inhibiting the catalytic activity of the clusters anymore. Corma *et al.*[31] even succeeded in depositing single gold atoms on carbon nanotubes. It appeared that these atoms had no activity in the aerobic oxidation of thiophenol. After a short induction period of 6 minutes, aggregation of the Au atoms has happened and the small nanoclusters (2-13 atoms) showed a high thiophenol conversion (~85%) after 1h. Finally, when the clusters aggregated into nanoparticles of diameter >1 nm, the catalyst activity dropped to zero. This sintering process results in the loss of activity and/or selectivity, mainly through a decrease in the number of exposed metal atoms but also through the alteration of their size-specific physical and chemical properties.[32,33]

Previous publications have shown numerous examples on the enhanced activity of gold particles upon alloying with another metal.[34,35] Recently, even bimetallic clusters have been synthesised in which one of the gold atoms is replaced by a palladium (Pd) atom.[36] Comparison in catalysis showed that single Pd doping of Au_{25} significantly improved its performance in various catalytic oxidations. There are two possible mechanisms by which the Pd atom can enhance the catalysis. One possible mechanism is that it directly creates a highly active reaction site on the surface of Au_{24} (the so-called "ensemble" effect).[37] Schiffrin reported that individual Pd atoms dispersed onto an Au NP host that acts as an electrocatalytic center for the oxygen reduction.[38] The other possible mechanism is that the Pd atom activates the Au sites by modulating the electronic structure (the so-called "ligand" effect).[37] It should, however, be noted that these synergistic effects between Au and a second metal strongly depend on the reaction and the conditions used. Another metal could strongly enhance the activity and selectivity of gold catalysts in one reaction while having no or even a negative effect in another reaction.

However, fundamental questions remain unanswered: How does the catalytic activity evolve in the nanosized regime? To answer this question, atomically controlled sizes of Au clusters must be synthesised and deposited on solid supports to prevent sintering. This sintering process results in the loss of activity and/or selectivity, mainly through a decrease in the number of exposed metal atoms but

also through the alteration of their size-specific physical and chemical properties.[32,33] It is, however, known that nanoparticles and clusters are more strongly bound on defect sites of the support material[39–41] leading to less aggregation, thus a more stable catalyst.

1.4 CeO_2 support material

Cerium oxide (ceria, CeO_2) is widely used in many areas of heterogeneous catalysis.[42] Among oxide catalysts, ceria has received a lot of attention due to its ability to switch between Ce^{3+} and Ce^{4+} oxidation states with a low redox potential.[43,44] and its high oxygen storage capacity.[45] In its various micro- and nanoparticle formulations, CeO_2 is fast gaining a reputation as a 'super-material' with applications in technical areas beyond heterogeneous catalysis, such as the fabrication of optical devices, fuel additives, mechanical polishing and solid oxide fuel cells.[46] For example, with a decrease in particle size of ceria, the energies for defect formation may be substantially reduced in nanocrystalline oxides, leading to markedly increased levels of nonstoichiometry and electronic carrier generation.[47]

The most common use of ceria is the metal/oxide configuration in which the stable, bulk ceria is used as a support material on which single crystals or metal nanoparticles can be deposited for an increased chemical activity.[48] It was found out that the physical and chemical properties of nanomaterials are not only sensitive to crystal size but also to crystal shape.[49] The oxide/metal configuration is also used in which single ceria crystals or well-defined oxide films are grown on top of a metal substrate or on another oxide. Even though these oxide/metals are less common in technical applications, they are quite useful for fundamental studies in catalysis.[50,51]

Several other studies with model ceria catalysts show the importance of strong metal-supports interaction.[42] For example: Alberto *et al.* have deposited gold nanoparticles (2-5 nm) onto nanocrystalline ceria (5 nm).[52] They showed that this catalyst was more active in the aerobic oxidation of 3-octanol if nanocrystalline CeO_2 is used as a support instead of larger, conventional CeO_2. Using in situ IR, they found out that bare ceria nanoparticles (before gold deposition) does oxidize alcohols to aldehydes in the liquid phase, consequently forming the cerium hydride. However, this cerium hydride is then not oxidized upon addition of O_2. This means that the reduced cerium is stable in the presence of physisorbed O_2 and the catalytic cycle is not closed. They proposed that the positive oxidation states of the gold nanoparticles are stabilised by creating Ce^{3+} and oxygen deficient sites in the ceria. This gold deposition also led to a disappearance of the cerium hydride and formation of water when oxygen was introduced. Their proposed mechanism for the liquid phase oxidation of alcohols based on Au-CeO_2 characterisation and IR study is shown in Figure 4. The interaction between Au and CeO_2 gives rise to an important population of positively charged Au and Ce^{3+} species, detectable by XPS (step 1). The alcohol or the corresponding alkoxide will then react with the Lewis acid sites of Au-CeO_2 to give a metal alkoxide (step 2), which subsequently undergoes a rapid hydride transfer from C-H to Ce^{3+} and Au^{+} to give the ketone product and stable Ce-H (indicated as LA-H) and Au-H (step 3). Upon addition of oxygen and coordination to the oxygen-deficient sites of CeO_2 (Ce^{3+}), formation of cerium coordinated superoxide species occurs (step 4). These superoxide species evolve into cerium hydroperoxide by hydrogen abstraction from Au-H (step 5), reforming the initial Au^0. Without Au, this last step would not be possible, thus lead to a depletion of Ce^{3+} formed in step 1.

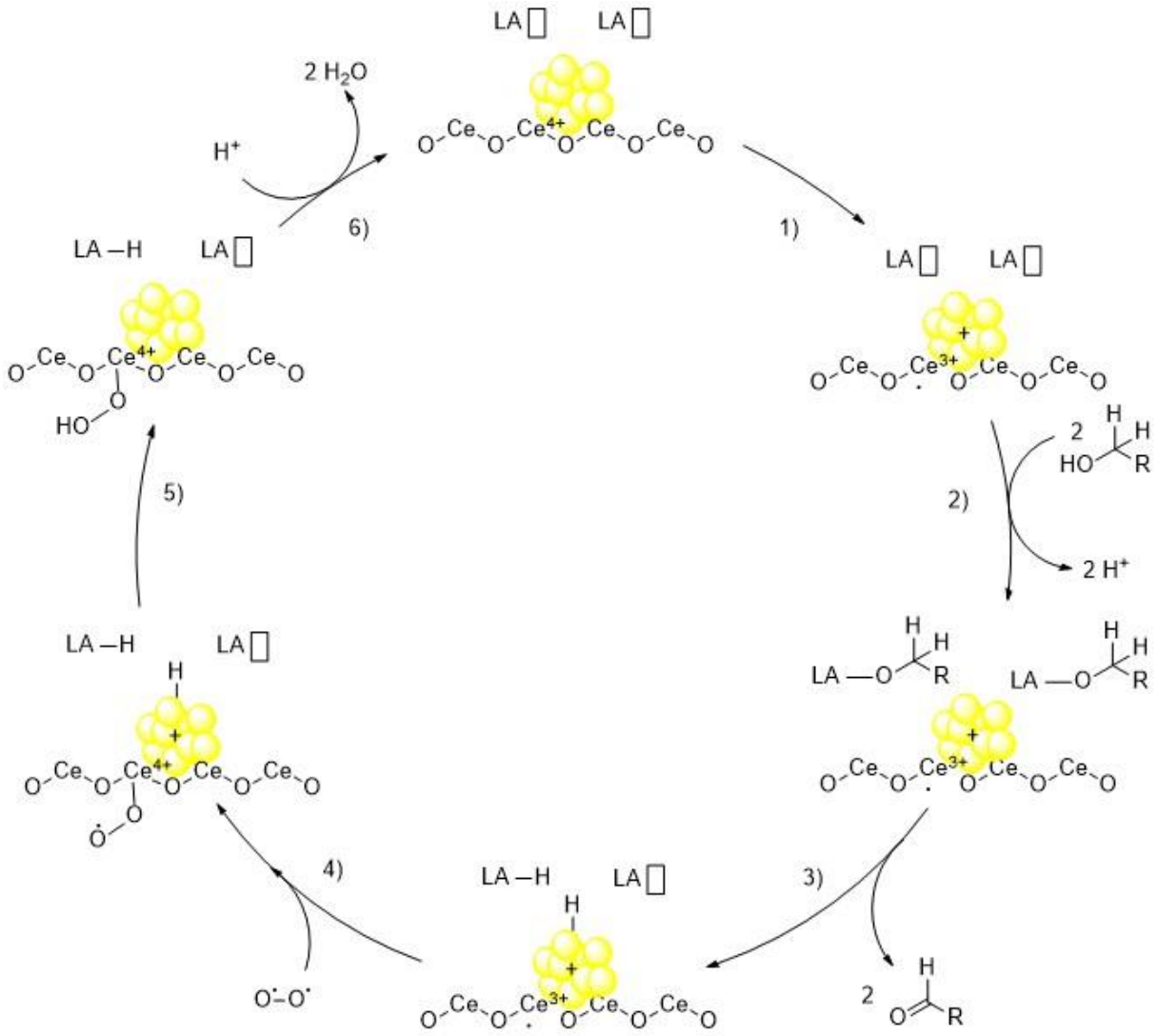

Figure 4. Proposed mechanism by Alberto *et al.*[52] for the liquid phase oxidation of alcohol on Au-CeO_2. LA = Lewis acid.

Late transition metal catalysts have also been reported to sinter more slowly or maintain smaller particles when supported on CeO_2 relative to other supports.[40,53,54] This could be due to the high amount of oxygen vacancies present on CeO_2 associated with its low redox potential between Ce^{3+} and Ce^{4+}.[43,44] Research done by Stephanopoulos and colleagues[55] revealed that gold nanoparticles deposited on CeO_2 nanorods are most active in CO oxidation compared to CeO_2 nanopolyhedra and nanocubes in that order. Other theoretical studies show that the formation energy of anion vacancies for different CeO_2 surfaces follows the order {110} < {100} < {111}.[56] This is associated with a high proportion of surface oxygen ions accommodating step/corner sites on {110} and {100} surfaces. The ions at these positions are more mobile and hence easier to extract, compared with oxygen ions on a {111} surface. This means that defects are most likely to be formed on {110} planes. This explains why the Au nanoparticles were more stable and reactive on ceria nanorods ({100} and {100} planes) compared to the nanopolyhedra ({110} and {111}) and nanocubes ({100}).[57]

CeO_2(110) (Figure 5a) is a surface with each layer having zero charge due to a stoichiometric balance of anions and cations in each plane. In CeO_2(111) (Figure 5b), each plane is charged but the repeat unit consists of three planes in a symmetrical configuration which leads to no net dipole moment perpendicular to the surface. The CeO_2(100) surface (Figure 5c) has alternately charged planes with a repeat unit of only two planes which produces a dipole moment perpendicular to the surface. This dipole moment can be eliminated in a straightforward way by removing half of the ions from one layer and move them to the opposing face as shown in Figure 5d.[58]

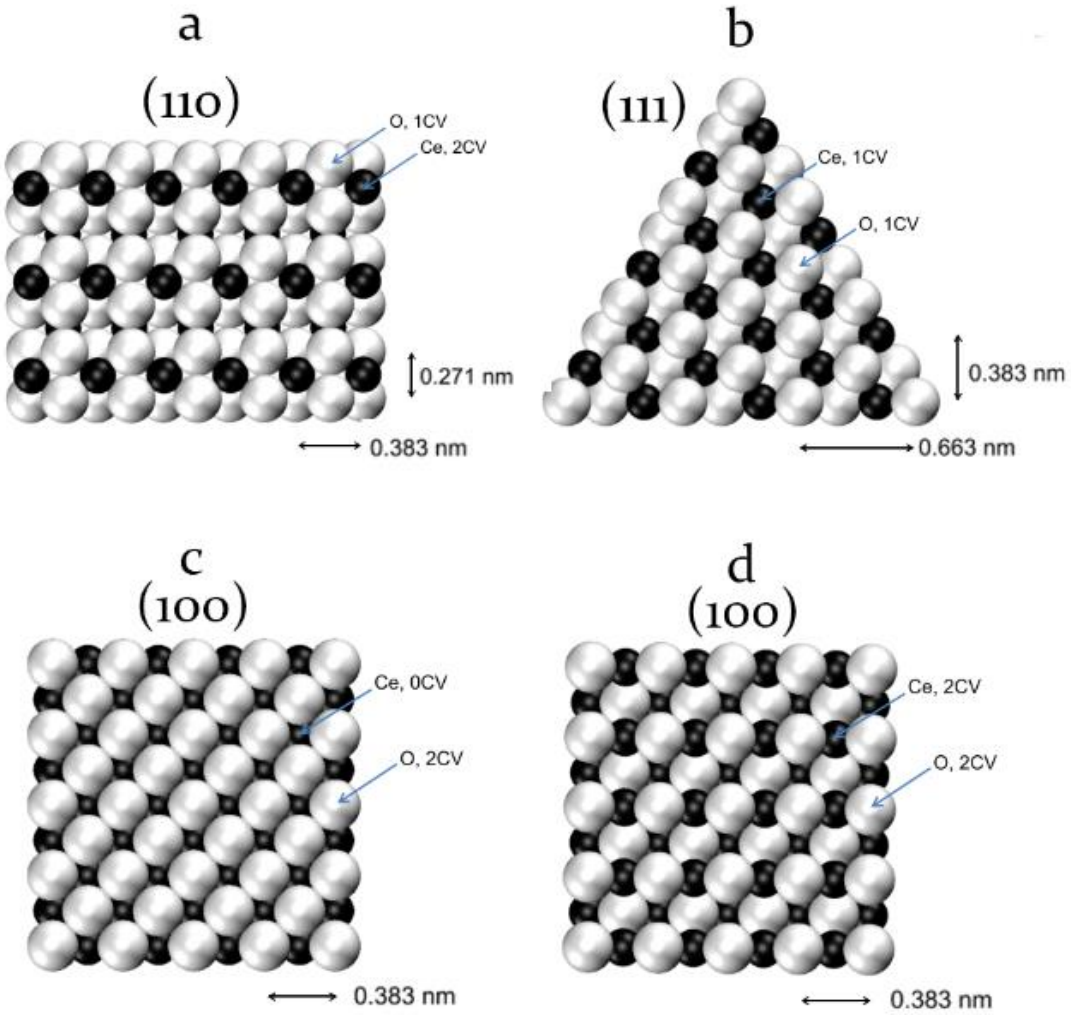

Figure 5. (a) CeO_2(110), (b) CeO_2(111), (c) CeO_2(100) and (d) CeO_2(100) depicted as reconstructed surface. The black spheres are Ce and the white spheres are O. The spheres have been drawn at 100% space-filling to indicate accessibility to subsurface sites. CV refers to the number of coordination vacancies around the Ce and O ions. Adapted from D. Mullins.[58]

The synthesis of these different ceria crystals has been widely studied.[57] A schematic diagram for the shape-selective synthesis of CeO_2 nanopolyhedra, -rods and -cubes is shown in Figure 6. Studies have shown that cerium forms $Ce(OH)_3$ nuclei upon reacting with a base such as OH^-. After a hydrothermal treatment of these nuclei in 0.01 M NaOH at 100°C for 24h, they were unchanged. However, when the NaOH concentration was further increased to 6 M, highly crystallized CeO_2 nanorods with a high aspect ratio are obtained due to the greatly accelerated dissolution/recrystallization under the high-base concentration. At the same high base concentration, as the temperature was further increased to 180°C, the dissolution/recrystallization associated with the hydrothermal treatment becomes more vigorous and results in CeO_2 nanocubes. It appeared that after 4 h, both cubic and rods were formed, but once the reaction time was longer than 8h, only nanocubes were yielded. It is suggested that at low NaOH concentrations (< 1 M) and a low temperature of 100°C the dissolution/recrystallization rate is slow and there might exist inadequately high chemical potential for driving the anisotropic growth of the $Ce(OH)_3$ nuclei. This results in CeO_2 polyhedra.

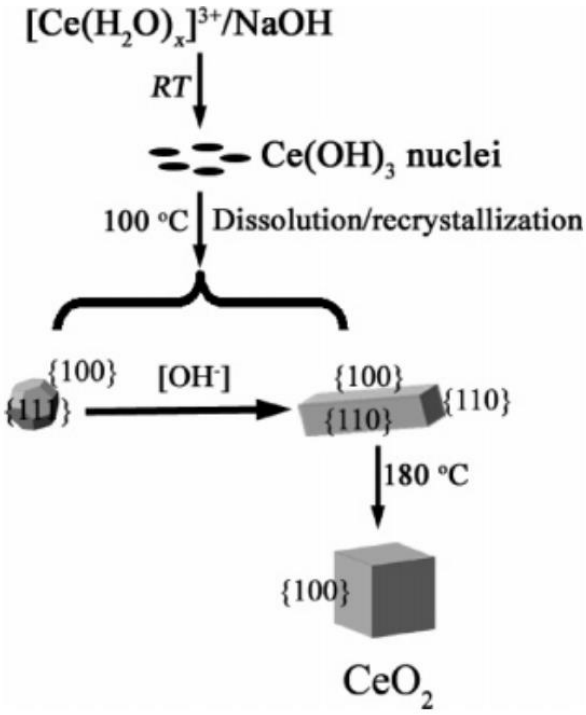

Figure 6. A schematic diagram of the shape-selective synthesis different of CeO_2 nanoparticles.

1.2 Goal of research

The goal of this research is to get an insight in the activity of Au containing clusters in the nanoscale. In order to do this, clusters must first be deposited on a (Lewis acidic) support. The protective ligands should be removed without causing sintering thus keeping the cluster atomicity unchanged. Hereafter, a model reaction can be chosen to investigate the activity of different clusters. This gives the following research questions:

1. Which exposed surface planes of CeO_2 are best at stabilizing Au clusters against sintering after heat treatment?
2. How do the selectivity and reactivity correlate to the Au cluster size and composition in a model oxidation reaction?
3. Can the protective ligands around phosphine stabilised clusters be removed using a chemical route instead of calcination?

1.3 Approach

Various clusters will be chemically synthesised (Au_9, Au_8, Au_8Pd and Au_6Pd). CeO_2 tends to stabilise small nanoparticles very well and it can remove ligands from clusters at a fairly low temperature, thus is chosen as a Lewis acidic support material. Different CeO_2 crystals with different exposed surface planes will be synthesised using hydrothermal treatment at varying temperatures and pH values. Afterwards, Au_9 clusters will be deposited on each crystal while maintaining the same number of clusters per nm. These samples will be heated and characterised to look for larger nanoparticle formation. Hereafter, the CeO_2 crystals which show the best stabilisation will be used as support material to further investigate the effect of cluster size (Au_9, Au_8) and composition (Au_8Pd, Au_6Pd) on the activity and selectivity in gas phase EtOH oxidation with O_2. Furthermore, Au_9 clusters will be deposited on SiO_2 and treated with a BCl_3 solution (strong Lewis acid) to chemically remove protective phosphine ligands (Lewis bases).

2. Theory

2.1 Diffuse Reflectance Ultraviolet-Visible spectroscopy

Ultraviolet-Visible spectroscopy (UV-Vis) refers to absorbance or reflectance spectroscopy in the ultraviolet-visible spectral region.[59] In this region of the electromagnetic spectrum, many molecules undergo electronic transitions, such as ligand to metal charge transfer (LMCT), d-d and π-π* transitions. This means that light with different energies can be absorbed depending on the structure of the material. One of the effects used for UV-Vis spectra is called diffuse reflectance (DR). This is the reflection of light or other waves/particles from a surface such that a ray on the surface is scattered at many angles rather than just one angle as in the case of specular reflection. DR UV-vis can be used to measure UV-Vis spectra of solid materials. A common characteristic of solid catalysts are their internal inhomogeneities. The propagation of light through such inhomogeneous material differs significantly from the propagation of light through more ordered, homogeneous material, since light scatters off points in its path. Therefore, a correction is needed to describe the propagation of light through these disordered materials. The most widely used model for diffuse reflectance is the so-called Kubelka-Munk (KM) function. This is a relatively simple solution in the case of semi-infinite samples. All the geometric peculiarities of the disordered sample are condensed into a single parameter, the scattering coefficient s. Once the absorbance of a sample is measured, the reflectance can be calculated using $R = 10^{-A}$. The diffuse reflectance (R_∞) in KM is given as:

$$R_\infty = 1 + \frac{k}{s} - \sqrt{\frac{k}{s}\left(2 + \frac{k}{s}\right)} \qquad \text{Equation 1}$$

Where k is the absorption coefficient of the sample: $k = 4\pi^k/_\lambda$ with λ as the wavelength yielding the KM absorbance:

$$KM = \frac{k}{s} = \frac{(1 - R_\infty)^2}{2R_\infty} \qquad \text{Equation 2}$$

The KM transform of the measured spectroscopic observable is approximately proportional to the absorption coefficient, and therefore is approximately proportional to the concentration. The KM absorbance can be retrieved using reflectance spectra and will give indications on the coordination environment of the species studied, such as transitions and geometry.

An important aspect of gold particles is their colour, which depends on their size and shape. This colour is caused by the so-called localised surface plasmon resonance (LSPR) effect. This effect originates from the collective oscillations of the conduction electrons in a particle. If light is used which photon frequency matches the natural frequency of the metal surface electrons, these conduction electron will start oscillating against the restoring force of their positively charged nuclei. Jin *et al.*[60] have shown that a "small" change in nanoparticle size of 33 atoms (Au_{246} → Au_{279}) gave rise to a LSPR band in UV-Vis around 520 nm. This indicated that gold particles smaller than ~2.3 nm do not possess this phenomenon. Furthermore, as particles become bigger, the LSPR band becomes more intense, broadens and shifts to higher wavelengths.[61] On the other hand, gold nanoclusters exhibit distinct optical features as a results of their differences in size, structure and bonding as they behave like some kind of metal molecules.[62]

2.2 X-ray diffraction

X-ray diffraction (XRD) is a technique used for determining the structure of crystalline materials. This method makes use of the fact that ordered atoms or molecules, as is the case in a crystalline phase, cause a beam of incident X-rays to diffract into many specific directions. By measuring the angles of these diffracted beams, crystalline phases can be assigned to certain materials via comparison of the diffraction pattern with databases. Sometimes, more than one phase is displayed in a diffractogram which can indicate the presence of another material (for example metal nanoparticles on an oxide support). This way, large nanoparticles can be observed (>3 nm in diameter) using XRD if the diffraction patterns of the metal and support material used do not overlap. Small crystals measured using XRD tend to have so called peak-broadening. This results in smaller particles displaying a broader peak in a diffractogram, whereas larger particles show a more narrow, intense peak.[63] This effect can for example subsequently be used to calculate the average particle sizes of the materials measured.

2.3 Transmission Electron Microscopy

Transmission electron microscopy (TEM) is a microscopy technique used for imaging various samples on nanoscale. Unlike a conventional microscope, TEM makes use of high-energy electrons, typically 30-200 kV, instead of visible light.[64] The wavelength of these electrons (∼1-10 pm depending on kV used) is smaller than that of visible light (380-780 nm) which makes it possible to image much smaller materials.

High-resolution TEM (HR-TEM) is simply a specialised TEM imaging mode that allows for direct imaging of the atomic structure of a sample. This way, the interplanar spacing between lattices can be measured with some precision. If the structure of the material is known, by using for instance XRD, the surface planes (h,k,l) corresponding to these interplanar spacings can be determined. For cubic systems, Equation 3 can be applied where d is the interplanar spacing measured in HR-TEM, a is the lattice constant of the unit cell and h, k and l are the miller indices corresponding to the plane.

$$\frac{1}{d^2} = \frac{h^2 + k^2 + l^2}{a^2} \qquad \text{Equation 3}$$

2. Experimental section

Chemicals: $CeNO_3 \cdot 6H_2O$ (Acros Organics, 99.5%), NaOH (EMSURE, ≥99.0%), CeO_2 nanopowder (Alfa Aesar, 99,5%, 15-30 nm, 50 m^2/g), PPh_3 (Acros Organics, 99%), $Pd(PPh_3)_4$ (Sigma-Aldrich, 99%, stored in fridge), CH_2Cl_2 (Acros Organics, 99+%, extra dry), methanol (VWR Chemicals, 99.9%), ethanol (VWR Chemicals, >99.5%), toluene (Acros Organics, 99.8+%), SiO_2 aerosil 300 (Degussa, fumed silica), hexane (Acros Organics 99+%), $HAuCl_4 \cdot 3H_2O$ (Sigma-Aldrich, ≥99.9%), dry CH_2Cl_2 (Acros Organics, 99.8%, extra dry, stabilised, AcroSeal), 1 M BCl_3 in CH_2Cl_2 (Acros Organics). All chemicals are used as received unless specifically mentioned otherwise. All H_2O used is milli-Q H_2O (22 °C, 18.2 MΩ·cm). All materials containing Au are protected from light and stored in a fridge.

2.1 Catalyst characterisation

For catalyst characterisation the following apparatus are used: UV-Vis (Lambda 950S coupled with a 150 mm InGaAs integrating sphere, Perkin Elmer), XRD (D2 Phaser 2nd Gen, Bruker, Co Kα radiation, λ = 1.79 Å measured from 20 to 80° 2θ, increment of 0.05° and step time of 1s), TEM and HAADF-STEM (Thermo Fischer Scientific Talos F200X at 200 kV equipped with a high-brightness field emission gun).

2.2 CeO_2 support synthesis

Different CeO_2 shaped crystals can be synthesised using a modified procedure obtained from Stephanopoulos *et al.*[55] A 120 mL Teflon tube was filled with H_2O (60 mL)and an appropriate amount of NaOH (see Table 1) was dissolved. $Ce(NO_3)_3 \cdot 6H_2O$ (1.94 g, 4.5 mmol) was dissolved in H_2O (30 mL) and dropwise added to the Teflon tube while stirring. This emulsion was stirred for 10 minutes and then sealed tightly in a stainless-steel autoclave. Hydrothermal treatment was carried out in an oven at different temperatures (see Table 1). After quenching the autoclaves, the white precipitates were collected, washed three times with H_2O and twice with ethanol and dried overnight at 120 °C. Afterwards, the yellow powders were calcined in air at 550 °C for 4h.

Table 1. Used conditions for obtaining different CeO2 crystals.

CeO_2 Crystal	NaOH (g)	T (°C)
Rods	21.6	100
Cubes	21.6	180
Polyhedra	0.36	180

2.3 Gold nanoclusters synthesis

2.3.1 $AuPPh_3NO_3$

$AuPPh_3NO_3$ can be synthesised following a previously described method obtained from Malatesta *et al*.[65] $AgNO_3$ (8.5 g, 50 mmol) dissolved in ethanol (200 mL) was mixed with a solution of $AuPPh_3Cl$ (10.0 g, 20 mmol) in CH_2Cl_2 (150 mL). Precipitated AgCl was filtered off after 30 minutes of stirring followed by solution evaporation to dryness. The solid was dissolved in chloroform and filtered from insoluble impurities. Finally, the solvent was removed using a rotary evaporator.

2.3.3 $AuPPh_3Cl$

$AuPPh_3Cl$ can be prepared according to the method described by Malvano *et al.*[66] An amount of $HAuCl_4 \cdot 3H_2O$ was dissolved in ethanol and a 2-fold excess of PPh_3 in methanol was added. A white precipitate of $AuPPh_3Cl$ was formed immediately. After 20 minutes the precipitate was collected by filtration, washed twice with ethanol and dried *in vacuo*.

2.3.4 $[Au_9(PPh_3)_8](NO_3)_3$

The cluster $[Au_9(PPh_3)_8](NO_3)_3$ (denoted as Au_9) was prepared by following a procedure proposed by Wen *et al.*[67] 0.072 g of $NaBH_4$ (0.072 g, 1.9 mmol) dissolved in ethanol (92 mL) was added to the magnetically stirred solution of $AuPPh_3NO_3$ (4.0 g, 7.67 mmol) in ethanol (160 mL). After two hours, the deep-red solution was filtered from insoluble impurities and evaporated to dryness. The solid was dissolved in CH_2Cl_2 (20 mL), filtered and evaporated on a rotary evaporator. The black solid was washed with tetrahydrofuran, and subsequently crystallized from methanol solution by slow diffusion of diethyl ether. Dark-green crystals, typical for an Au_9-cluster formed within 5 days.

2.3.5 $[Au_8(PPh_3)_8](NO_3)_2$

The cluster $[Au_8(PPh_3)_8](NO_3)_2$ (denoted as Au_8) was synthesised from Au_9 following the procedure by Van der Velden *et al.*[68] Au_9 clusters (0.371 g, 0.091 mmol) and PPh_3 (0.243 g, 0.93 mmol) were mixed in CH_2Cl_2 (5 mL). The solution was stirred for 30 minutes. The red solid was precipitated by adding toluene (75 mL), isolated by filtration and washed with toluene three times. The Au_8 crystals were grown from CH_2Cl_2 solution by slow diffusion of diethyl ether. After 5 days, red crystals (0.306 g) were formed and the solution turned colourless. Yield 0.118 g (88%). The cluster was characterised using UV-Vis spectroscopy (Figure S1) and matched with earlier reported data.

2.3.6 $[Au_8Pd(PPh_3)_8]Cl_2$

The cluster $[Au_8Pd(PPh_3)_8]Cl_2$ (denoted as Au_8Pd) was prepared following a procedure proposed by Tsukuda *et al.*[69] First, $AuPPh_3Cl$ (0.142 g, 0.29 mmol) and $Pd(PPh_3)_4$ (0.133 g, 0.12 mmol) were dispersed in ethanol (12 mL). To this yellow solution, a solid form of $NaBH_4$ (0.0152 g, 0.40 mmol) was added slowly over 10 min. After stirring for 1h, the reaction mixture was poured into hexane (200 mL) to form a precipitate. The precipitate was collected by centrifugation, washed with hexane and pure water, and extracted with ethanol. The solid product was obtained by evaporating the solvent. The solid and PPh_3 (0.196 g, 0.37 mmol) are dissolved in ethanol (10 mL) and the mixture is stirred for 1.5 h. The precipitate that formed upon adding hexane was then again collected by centrifugation, washed with hexane, and extracted with ethanol. The solid product was obtained by evaporating the solvent. Yield 0.108 g (77% with respect to Au). The cluster was characterised using UV-Vis spectroscopy (Figure S2) and ^{31}P-NMR (CD_3CN: δ 51.6 (s) ppm, Figure S3) and matched earlier reported data.

2.3.7 $[Au_6Pd(PPh_3)_7](NO_3)_2$

The cluster $[Au_6Pd(PPh_3)_7](NO_3)_2$ (denoted Au_6Pd) was synthesised according to the method described by Quintilio *et al.*[70] First, a 100 mL round-bottom flash was filled with $PdCl_2(PPh_3)_2$ (0.30 g, 0.43 mmol) and $AuPPh_3NO_3$ (1.08 g, 2.00 mmol) in CH_2Cl_2 (10 mL) with stirring. $NaBH_4$ (0.039 g, 1.03 mmol) was dissolved in ethanol (10 mL) and added dropwise to the metal precursor solution. The dark red solution was stirred at room temperature for 30 min and then H_2O was added to quench the reaction. The solvents were removed under vacuum and methanol was added to the flask. The crude mixture was filtered through Celite-545 on a fritted glass funnel to remove insoluble precipitate. The dark red filtrate was evaporated until dry and acetone (20 mL) was added to the solid. The resulting solution was again filtered and the filtrate was evaporated to dryness using a rotary evaporator. The product was dissolved in methanol (5 mL) and precipitated by the addition of diethyl ether (40 mL). The dark brown solid was centrifuged and dried *in vacuo*.

2.4 Cluster deposition

1 g of support material (CeO_2 or SiO_2) was suspended in a mixture of methanol (2.5 mL) and CH_2Cl_2 (15 mL) and sonicated for *ca.* 30 minutes. Appropriate amount of cluster was dissolved in CH_2Cl_2 and added dropwise to the support suspension under vigorous stirring. After 15 minutes of stirring, toluene (10 mL) was added to the suspension in order to enhance cluster deposition. Hereafter, the solvents are evaporated using a rotary evaporator until a thick slurry of cluster/support is formed. To the formed slurry a small volume of CH_2Cl_2 was added and briefly stirred until homogeneous and the solvents were evaporated again until dry.

2.5 Au_n-CeO_2

Au nanoparticles can be deposited on CeO_2 by deposition precipitation following a procedure by Rodriguez *et al.*[71] CeO_2 (0.5 g) was sonicated in H_2O (25 mL) for 10 minutes. Then, 1 M $(NH_4)_2CO_3$ (12.5 mL) was added while stirring. $HAuCl_4 \cdot 3H_2O$ solution (0.029 mmol, 5.7 mg in 12.5 mL) was added dropwise and stirred for 1h while the pH of this solution was kept at 8-9 using 1M $(NH_4)_2CO_3$. Hereafter, the precipitate was filtered, washed 3 times with H_2O at 70 °C and dried *in vacuo* at 70 °C overnight. The product was calcined in static air at 400 °C for 4h.

2.6 Chemical ligand removal

SiO_2 containing deposited Au clusters (0.5 g) was dried *in vacuo* overnight at room temperature. Dry CH_2Cl_2 (20 mL) was added under N_2 atmosphere and stirred for 30 minutes. Afterwards, an excess of 1 M BCl_3 in CH_2Cl_2 (0.5 mL) was added and stirred for 1 h. The colourless powder was obtained, washed with dry DCM three times using inert filtration and dried *in vacuo*.

2.7 Catalytic experiments

To study the catalysts for ethanol oxidation, 50 mg of catalyst (90-150 µm) was diluted with 150 mg SiC (212-450 µm). The catalysts were used as synthesised without any pre-treatment. Helium was bubbled at a rate of 4.8 mL min^{-1} through a saturator maintained at 34 °C containing ethanol. This gas mixture was subsequently diluted with O_2 (1.25 mL min^{-1}) and more He (35.7 mL min^{-1}). This produced an ethanol/O_2 reactant mixture of 1:2 and total flow of 41.7 mL min^{-1}. GHSV = 50.000 mL g^{-1} h^{-1}. The temperature of the catalyst was controlled by a furnace and monitored by an internal thermocouple. A portion of the product stream was extracted periodically with an automatic sample valve and analysed using a Compact 4.0 gas chromatograph with a RT-Q-Bond (10 m, 0.32 mm in diameter). A schematic representation of the catalytic set-up is shown in Figure 7.

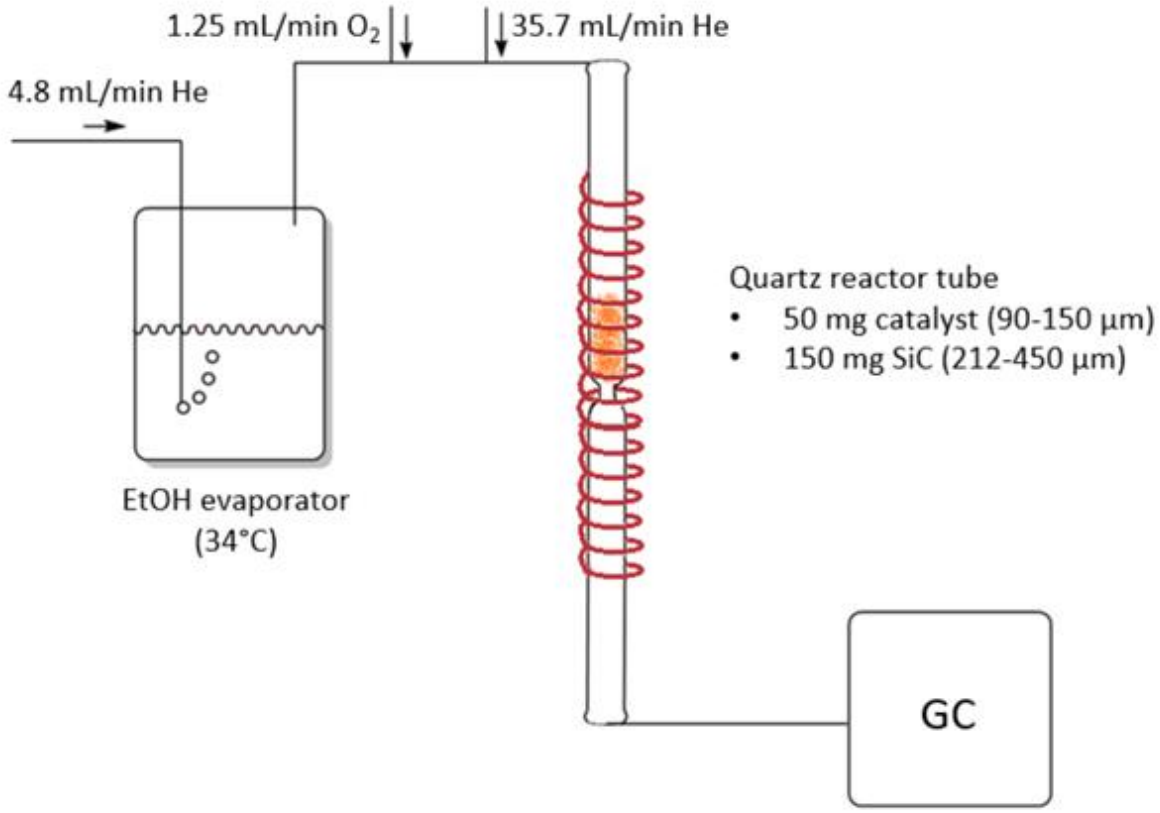

Figure 7. Schematic representation of catalytic oxidation setup.

3. Results and Discussion

3.1 CeO_2 crystals characterisation

The phase structure of the synthesised CeO_2 crystals is identified by XRD characterisation shown in Figure 8. All of the diffraction peaks in the XRD patterns could be indexed to the cubic fluorite structure of CeO_2 with Fm-3m space group (JPCDS 34-0394). The broad signals for the polyhedra and rods shown their nanocrystalline nature while the more narrow signals for cubes indicate these crystals are larger and consist of no microstrain.[72]

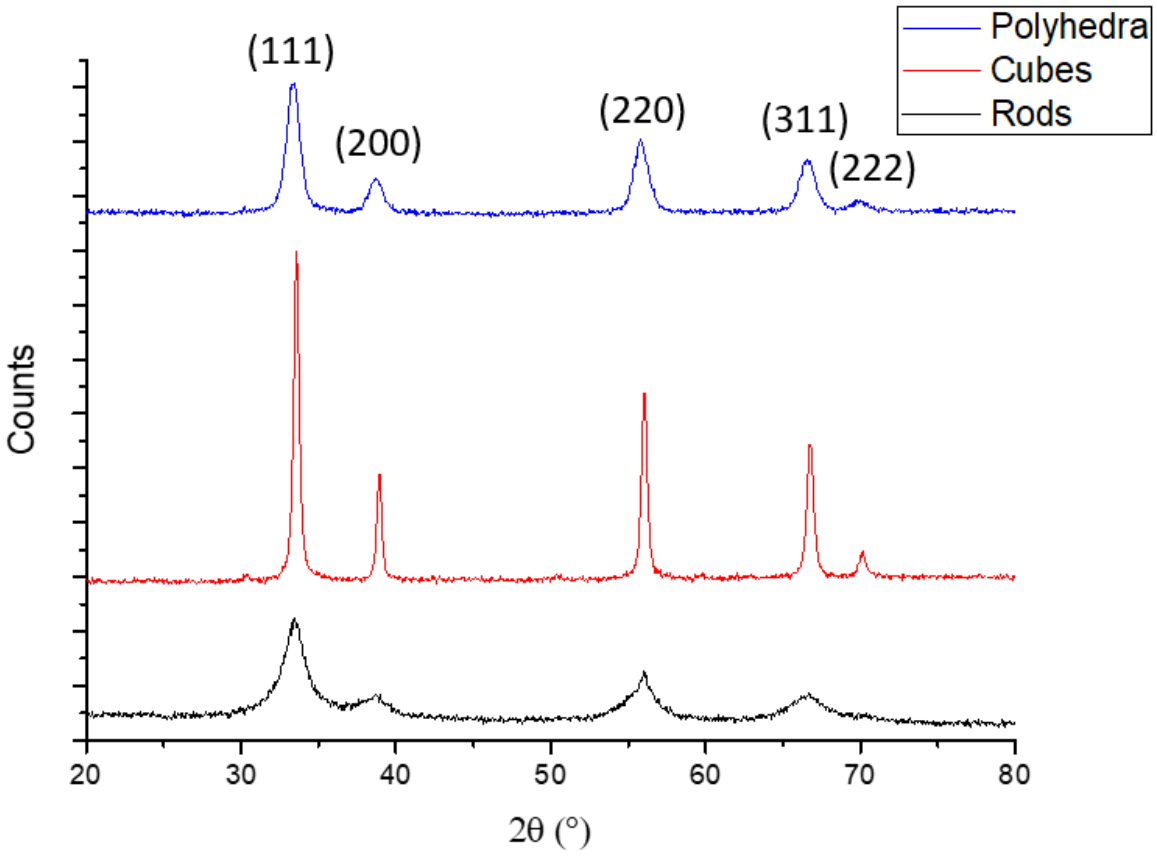

Figure 8. XRD diffractogram of CeO_2 rods (black), cubes (red) and polyhedra (blue).

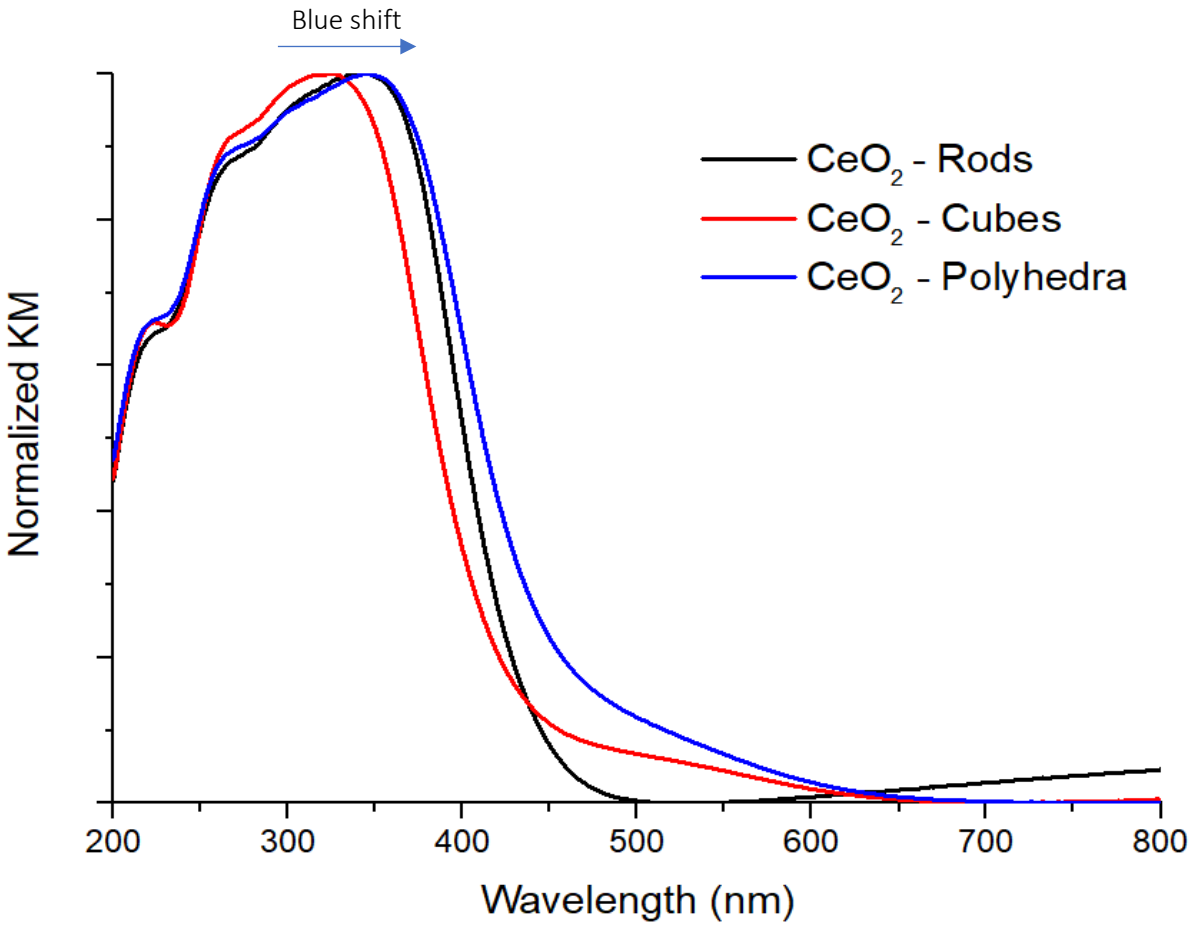

Figure 9. UV-Vis spectra of CeO_2 rods (black), cubes (red) and polyhedra (blue).

Figure 9 shows the measured UV-Vis spectra of each synthesised CeO_2 material. The adsorption band around 350 nm represents the band gap in CeO_2 nanoparticles.[73] The adsorption edge of both CeO_2 rods and polyhedra is blue shifted compared to that of CeO_2 cubes. It has already been shown in literature that the band gap increases for decrease in particle size as bulk CeO_2 tends to have a larger band gap than nanosized CeO_2 (called quantum size effect).[74] However, Figure 8 suggests that the CeO_2 cubes are smaller than the CeO_2 rods and polyhedra, thus it should have the smallest band gap which it does not. Other research has shown that the blue shift is due to the valence change of the Ce ions rather than the quantum size effect.[75] They said that the change from Ce^{4+} to Ce^{3+} increases the charge transfer gap between O 2p and Ce 4f band. This suggests that the blue shift in Figure 9 originates from CeO_2 cubes and rods exhibiting more Ce^{3+} ions on its surface which means that their surfaces are more easily reduced compared to CeO_2 polyhedra.

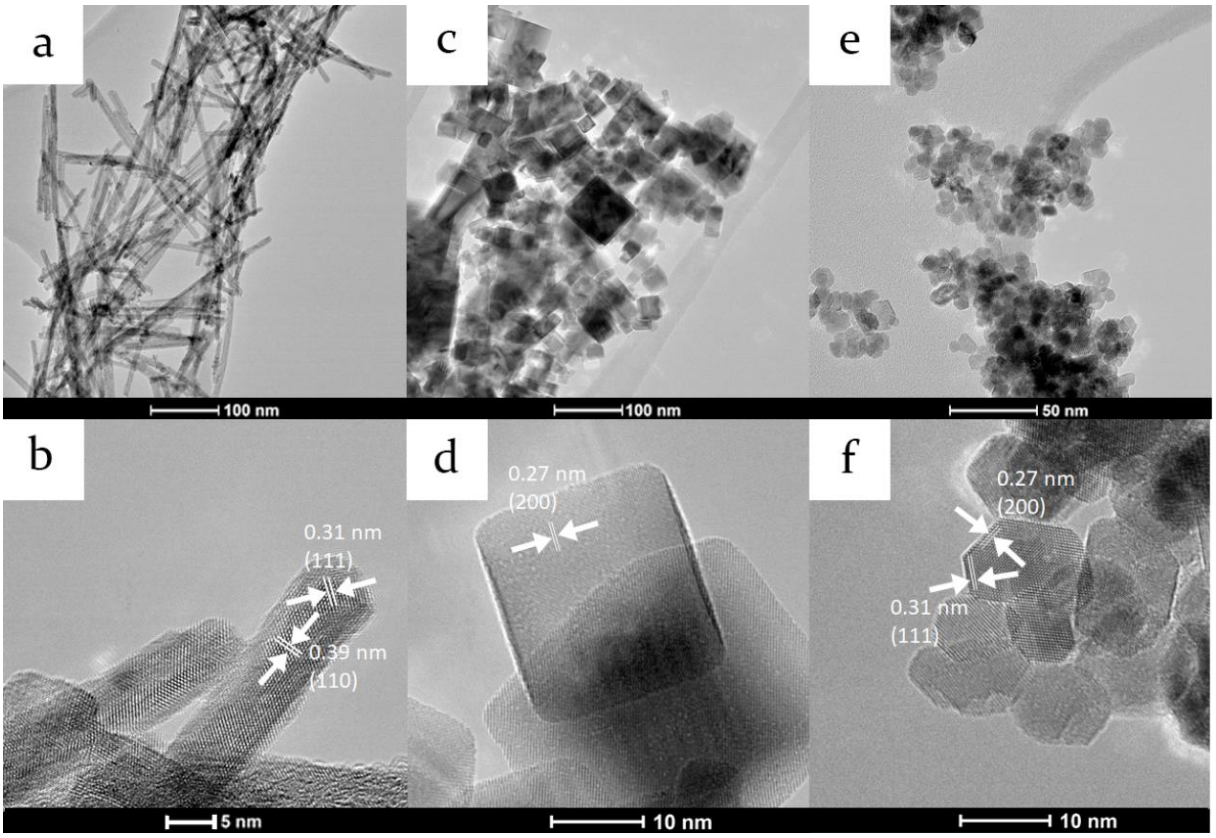

Figure 10.TEM and HRTEM images of CeO_2 rods (a,b), cubes (c,d) and polyhedra (e,f).

TEM and HRTEM images of each CeO_2 are shown in Figure 10. The interplanar spacings are measured using the HRTEM images. XRD confirms a cubic structure for each CeO_2 crystal, so Equation 3 can be used to determine their corresponding exposed surface planes. Figure 4b displays interplanar spacing of 0.39 nm and 0.31 nm for the CeO_2 rods (CeO_2-R) corresponding to {110} and {111} exposed planes respectively. The interplanar spacing of 0.27 nm in Figure 4d indicates the presence of {100} surface planes on CeO_2 cubes (CeO_2-C). Finally, the interplanar spacing of 0.31 nm and 0.27 nm display {111} and {100} exposed planes on CeO_2 polyhedra (CeO_2-P). Even though earlier discoveries do not always agree on the same exposed planes for each crystal, these results have indeed been previously reported.[72,76]

In another experiment, the $Ce(NO)_3{\cdot}6H_2O$ salt was directly added to the NaOH solution while maintaining the same final concentrations as previous experiments. This resulted in no formation of CeO_2 nanorods which maintained their small nanoparticle size (Figure S4a) and larger CeO_2 cubes (Figure S4b) which is unwanted due to their low surface area. This stresses the importance of first dissolving the Ce^{3+} source and adding it dropwise to the NaOH solution.

In order to obtain longer, well defined nanorods it is also important to slowly cool down the autoclaves after hydrothermal treatment (preferably overnight). If quickly quenched, the small CeO_2 nuclei may not have enough time to fully grow into nanorods (Figure S5). These quickly quenched rods may have a more rough surface and black dots suggesting there are many defects which may better stabilise nanoparticles.[77,78] However, for the sake of this project, all other synthesised nanorods are slowly cooled down to better investigate the effect of surface planes on the sintering of nanoparticles.

Finally, the BET surface areas of each CeO_2 materials is measured and shown in Table 2. This confirms the larger particles size for CeO_2 cubes measured using XRD as they possess a lower BET surface compared to CeO_2 rods and polyhedra.

3.2 Heat treatments of Au_9-CeO_2

After measuring the BET surface area of each crystal, Au_9 clusters were deposited on them. Their Au loading was measured using ICP-AES and shown in Table 2. Even though the Au loadings vary among the samples, their number of clusters per nm is close to identical. This way, the stabilising properties of exposed surface planes against Au clustering can be better investigated.

Table 2. Physisorption and ICP-AES data of ceria crystals containing Au_9 clusters

CeO_2 crystal	BET surface area (m^2/g)	Au loading (wt%)	Cluster loading ($*10^{-2}$ nm^{-2})
Rods	98.8	0.41	1.42
Cubes	35.5	0.14	1.34
Polyhedra	88.6	0.36	1.45

These Au_9 on CeO_2 samples (Au_9-R for rods, Au_9-C for cubes and Au_9-P for polyhedra) are heated to 120 °C for 4h in static air. Their UV-Vis spectra before and after treatment are shown in Figure 11. Even though the adsorption of the Au_9 cluster and CeO_2 largely overlap, it can be noted that after treatment some of the typical Au_9Figure S2 absorption bands (around 300 nm) are lost. This indicates a change in their electronic structure, thus a removal of PPh_3 ligands around the Au core.[79]

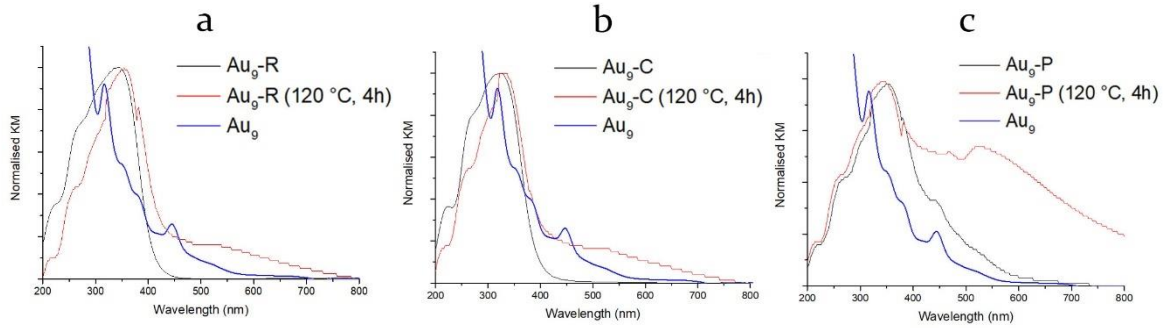

Figure 11. UV-Vis spectra of Au_9-R (a), Au_9-C (b) and Au_9-P (c) before (black) and after heat treatment at 120 °C for 4h (red). Note that the spectrum of Au_9 clusters (blue) is measured dissolved in ethanol and does not possess the same y-axis but is still added for clarity.

Hereafter, the Au_9-CeO_2 samples are also heated at 350 °C for 4h under 30:70 H_2:N_2 mixture gas flow to induce oxygen vacancy formation. For better comparison, Their UV-Vis spectra of the samples after both heat treatments are shown in Figure 12. The broader and intense absorbance band around 520 nm indicates the presence of more and larger nanoparticles in Au_9-P after both treatments. Figure 12b shows a higher adsorption band at 520 nm for Au_9-R compared to Au_9-C. This does not necessarily mean that Au_9-R contains larger particles as it had a higher Au loading (see Table 2), thus more Au particles that might absorb the light per gram of sample.

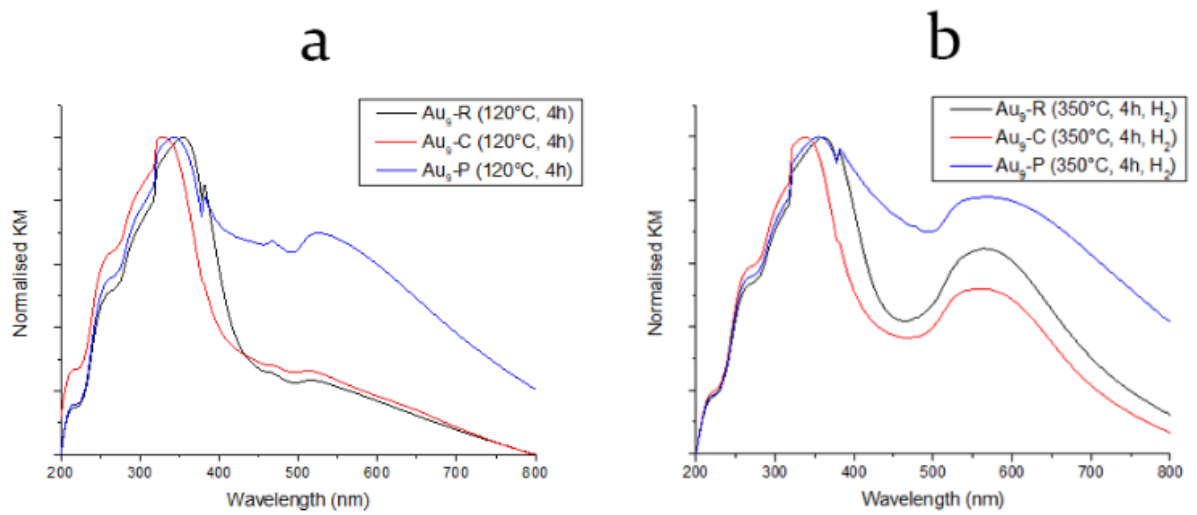

Figure 12. UV-Vis of Au_9-R (black), Au_9-C (red) and Au_9-P (blue) after heat treatment at 120 °C for 4h in air (a) and 350 °C for 4h under 30% H_2 flow (b).

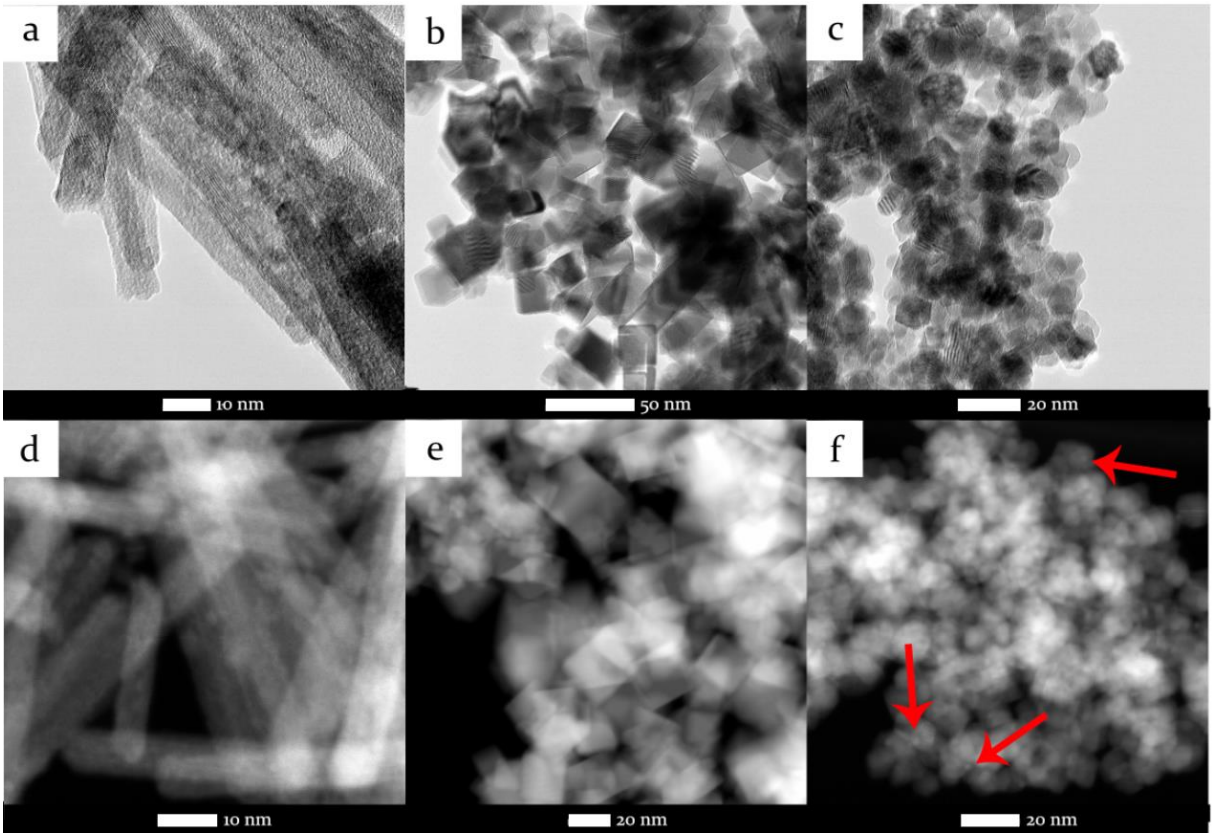

Figure 13. TEM images of Au_9-R (a), Au_9-C (b), Au_9-P (c) and HAADF-STEM images of Au_9-R (d), Au_9-C (e), and Au_9-P (f).

TEM and HAADF-STEM images of the Au_9-CeO_2 samples heated to 120 °C are shown in Figure 13. There is no clear sign of nanoclusters or nanoparticles in any of the samples. This might be due to the small size of the clusters and small contrast in STEM between Au and Ce because both elements have a relatively high atomic number. However, Figure 13f does indeed show some small nanoparticles as indicated by the UV-Vis spectra in Figure 12b.

Combining these UV-Vis and TEM results, we can conclude that the Au_9 clusters barely grew in size on the CeO_2 rods and cubes, and the polyhedra are least suitable for cluster stabilization. This means that exposed {100} and {110} planes are better at stabilising nanoclusters compared to {111}. This can be due to the fact that {111} is the most stable surface plane which is least favoured in oxygen vacancy generation, while this is easier on the less stable {100} and {110} planes.[80,81]

3.3 Catalytic oxidation of ethanol

Firstly, it should be noted that all catalytic tests are done on materials without any pre-treatment unless specifically said otherwise. The first catalytic test is done on pure CeO_2 rods without gold at different temperatures to test its activity. Its mayor products are acetaldehyde (AA) and CO_2, but trace amounts of CO and acrolein are also detected. The ethanol conversion is defined as: $yield_{AA}$ (%) + $yield_{CO2}$ (%).

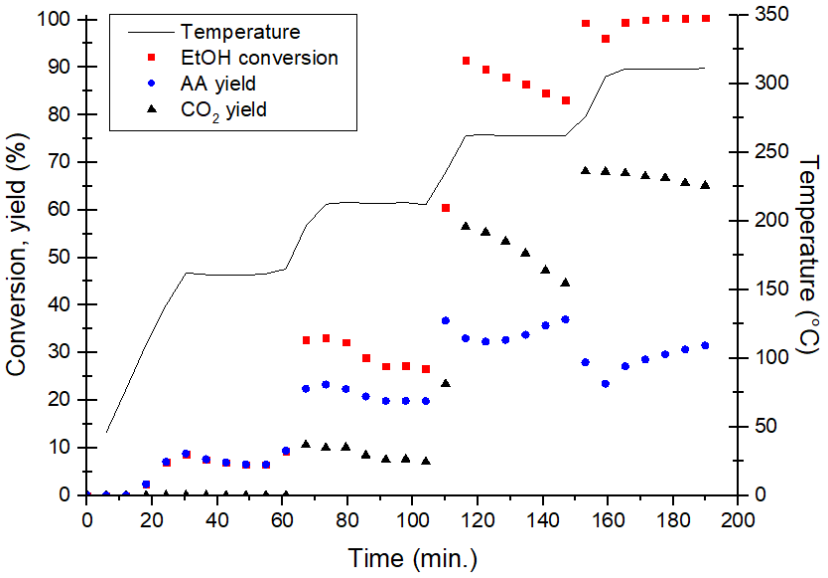

Figure 14. Ethanol conversion (red), acetaldehyde yield (blue) and CO_2 yield (black) in ethanol oxidation using CeO_2 rods.

It appears in Figure 14 that at low temperatures (150 °C) the only product formed is acetaldehyde (Equation 4) while at higher temperatures CO_2 is also formed corresponding to the combustion of ethanol (Equation 5). It can be seen that at each temperature the conversion decreases over time which could be due to the decrease in surface oxygen and absence of gold[52] or poisoning of the support, which will be looked more into later in this research. This deactivation is not present at very high temperatures (300 °C) because at those conditions the ethanol and oxygen can spontaneously form acetaldehyde without a catalyst (Figure S6).

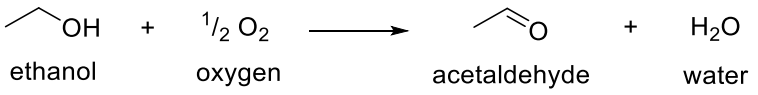

Equation 4

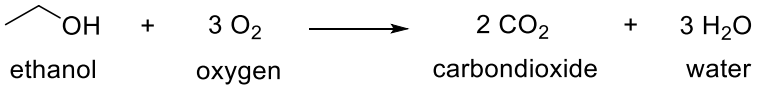

Equation 5

Hereafter, the activity of CeO_2 cubes and Au_9-C is tested and their results are shown in Figure 15. The low Au loading of 0.13 wt% used in Figure 15a is the same as used in stability experiments (see Figure 12) to minimize sintering of the clusters. However, this low loading also results in difficulty in determining the activity of the clusters. The differences in activity between the CeO_2 cubes with and without Au_9 clusters are slight, especially at lower temperatures (150 °C). Increasing the Au loading does not contribute well to the activity as it strangely only decreases (Figure 15b). This is why other cluster composition and size effects were investigated on CeO_2 rods since these are more suitable for higher Au loadings. Furthermore, Figure 15b shows no clear activation or increase in activity at 150 °C so it could be assumed that all protective ligands are dislodged from the Au_9 core at this temperature.

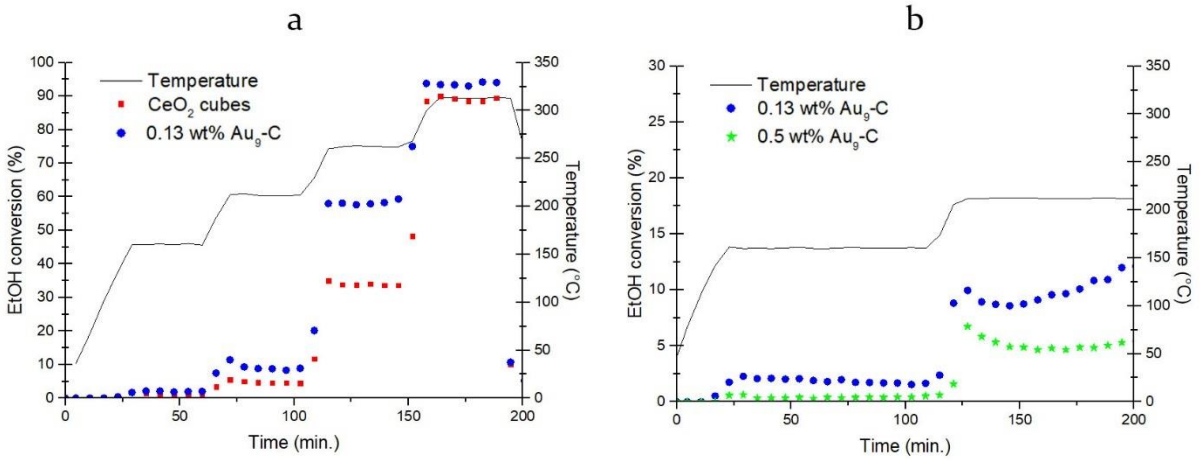

Figure 15. Temperature dependant ethanol conversion over CeO_2 cubes (red), 0.13 wt% Au_9-C (blue) and 0.5 wt% Au_9-C (green).

Au_9 and Au_8Pd clusters are deposited on CeO_2 rods (called Au_9-R and Au_6Pd-R) with metal loadings of 0.61 wt% Au and 0.42 wt% respectively and their results in EtOH oxidation are shown in Figure 16. First of all, it seems in Figure 16a that a conversion larger than 100% is measured which is, of course, impossible. This is because the evaporator did not maintain a single stable temperature and varied between 33 °C and 35 °C. This makes is difficult to calibrate ethanol concentrations on the GC, so it is assumed in all graphs that the vol% ethanol in the gas feed mixture is 1.49% based on the vapor pressure calculation.

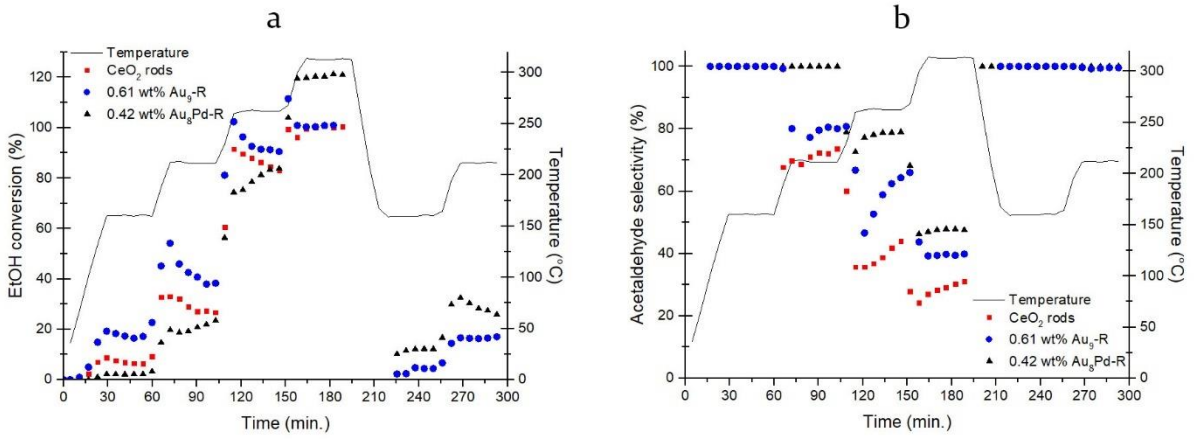

Figure 16. Temperature dependant ethanol conversion (a) and acetaldehyde selectivity (b) over CeO_2 rods (red), Au_9-R (blue) and Au_8Pd-R (black).

It is clear that the Au_8Pd clusters are less active compared to bare CeO_2 rods and Au_9 at lower temperatures in Figure 16a. However, around 200 °C and 250 °C, these bimetallic clusters seem to activate resulting in more EtOH conversion compared to Au_9 cluster. This higher activity is in line with previous beliefs of bimetallic nanoparticles having higher activities.[34,36,82] This increase in conversion of Au_8Pd around 250 °C might be explained due to stronger bound ligands to the Au cores because of the presence of either Pd or Cl^- anions (instead of NO_3^-). To further test this hypothesis, a small vial containing the Au_8Pd cluster is put in a 120 °C oven for 4h. This resulted in no colour change which did change for Au_9, Au_8 and Au_6Pd clusters. This might indicate that no alternation in electronic structure happens after this treatment for the Au_8Pd cluster and possibly no removal of ligands below 120 °C.

Figure 16b also shows that the selectivity towards acetaldehyde increases upon the addition of Au_9 clusters to ceria and is even higher with the use of bimetallic Au_8Pd clusters.

After treatment at 300 °C, Figure 16a shows a rather low EtOH conversion for Au_9-R, even lower than for the bare CeO_2 before this treatment at the same temperatures. The Au particles have grown to larger sizes (4.1 ± 1.3 nm, Figure S7) which could conclude that these particles are less active in the activation of oxygen, but this might not be the only reason for deactivation as shown in later experiments. It should, however, be noted that these particle sizes are measured on another microscope with a lower resolution resulting in no appearance of small particles so their actual average Au particle size could be lower.

Au nanoparticles are grown on ceria rods using deposition precipitation (called Au_n-CeO_2). Its UV-Vis spectra and TEM results are shown in Figure S8 and Figure S9 respectively. Even though the TEM images show no nanoparticles, a small LSPR band in UV-Vis indicates the presence of small nanoparticles. Au_6Pd and Au_8 clusters are also deposited on CeO_2 rods. The results of these catalysts in ethanol oxidation are shown inFigure 17.

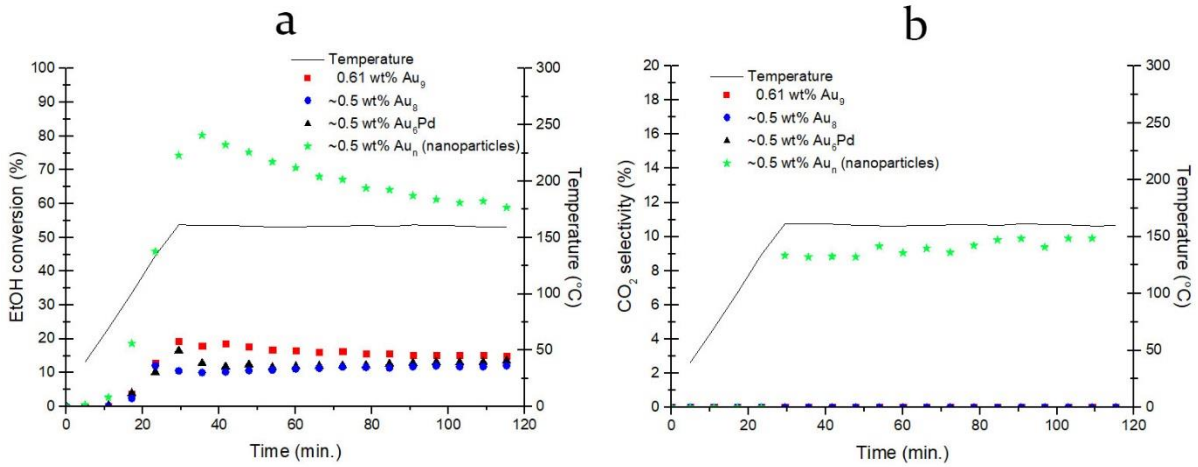

Figure 17. Time dependant ethanol conversion (a) and CO_2 selectivity (b) over Au_9-R (red), Au_8 (blue), Au_6Pd (black) and Au_n nanoparticles (green) on CeO_2 rods.

Au_n nanoparticles are much more active in ethanol oxidation compared to all used clusters, despite its lower number of exposed surface metal atoms. This might be a result of the calcination step used in Au_n-CeO_2 synthesis. This could have led to a closer interaction between Au and CeO_2 (depicted in Figure 18). The metal-CeO_2 interface is often considered to be the active site in these kind of oxidation reactions[48,81,83] as is also shown in Figure 4. It could also be the case that the NO_3^- counter anions in clusters have a negative effect in catalytic activity as shown before in literature for both Au_9 and Au_8.[28]

Upon close investigation of Figure 17, it seems that the Au_8 cluster sample activates from 30 minutes onwards as its EtOH conversion increases (due to possible removal of protective ligands around the Au_8 core). Furthermore, the EtOH conversion for Au_6Pd clearly decreases between 30-40 minutes into the reaction indicating deactivation. The Au_9 clusters do indeed sinter in at these reaction conditions (Figure S10) meaning the other clusters might too. This is why the turnover

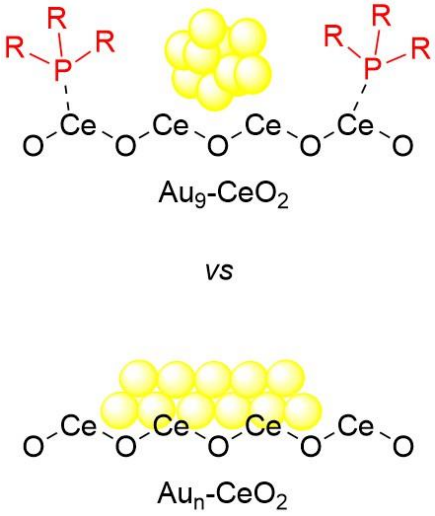

Figure 18. Representation of the possibly different interactions between Au and CeO_2 in Au_9-CeO_2 and Au_n-CeO_2.

frequencies (TOFs) of each catalyst are calculated (using Equation S1 and Equation S2) after 36 minutes in the reaction to neglect any cluster aggregation or deactivation. These TOFs, as well as metal loadings obtained from ICP, are shown in Table 3.

Table 3 Catalyst ICP results and TOF after 36 min.

Cluster	Metal loading (wt%)	TOF (mol_{EtOH} mol_{Au}^{-1} h^{-1})
Au_9	0.61	93.4
Au_8	~0.5	28.2
Au_6Pd	~0.5	52.5
Au_n	~0.5	671

As only ICP results are known for the Au_9-R sample, all other metal loadings are expected to be 0.5 wt% deduced from calculations. Table 3 clearly shows the highest activity for Au_n nanoparticles. Au_8 clusters are visibly the least active in EtOH oxidation. This could be explained by the fact that Au_8 has an even number of valence electrons and thus paired electrons which are less active in catalysis.[15] Also, Au_8 has a higher HOMO-LUMO gap compared to Au_9 as a result of the so-called odd-even oscillation effect in Au clusters.[14,16,84] This would explain the lower activity in EtOH oxidation if O_2 activation by Au is expected to be the rate determining step. Additionally, the bimetallic Au_6Pd cluster does not have a significant higher activity compared to Au_9 clusters which was contrary to what was expected in previous studies. This might indicate that bimetallic particles do not increase the activity as this catalytic reaction has another mechanism compared to the ones studied earlier.

Another remarkable result is that the Au_n catalyst significantly deactivates over time whereas this is less the case for the catalysts prepared from clusters. Even though TEM images don't show the presence of larger particles after catalysis for Au_n particles (Figure S11), their colour change measured using an UV-Vis CRAIC microspectrophotometer reveals a large LSPR band indicating particle growth (Figure 19). This can explain the deactivation to some extent.

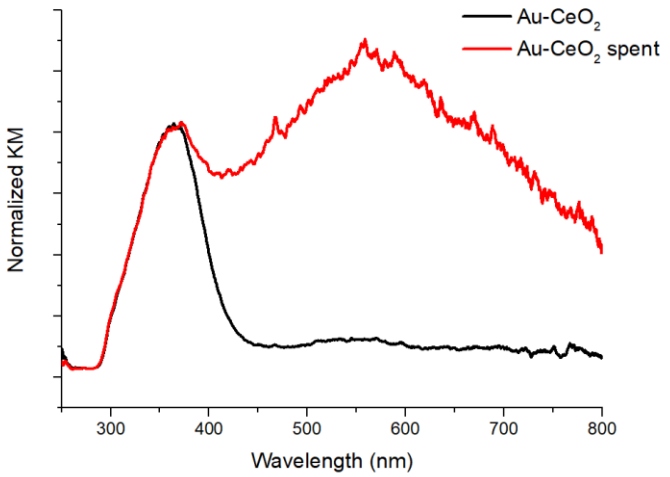

Figure 19 UV-Vis spectra of Au_n-CeO_2 before (black) and after (red) EtOH oxidation at 150 °C for 4h measured on a CRAIC microspectrophotometer.

Figure 17b shows that the nanoparticles also form CO_2 besides acetaldehyde whereas the clusters do not. The increased deactivation may thus originate from chemisorbed CO_2 species (mono-, bi-, poly-dentate and hydrogen carbonate species) which block the active sites.[83,85,86] To confirm this, FT-IR spectra of CeO_2 rods, Au-CeO_2 and spent Au-CeO_2 are measured and displayed in Figure 20. The band around 1330 cm^{-1} can be described by an N-O stretch leftover after CeO_2 synthesis which disappears after catalysis.[87] Furthermore, the band around 1433 cm^{-1} that originates after catalysis does indeed represent C-O stretch of polydentate carbonate bound to the CeO_2 surface.[86] This hypothesis could be further proven by a carbon balance below 100%. However, due to the fluctuation in temperature of the evaporator, the precise ethanol content could not be calibrated which made it impossible to calculate a carbon balance.

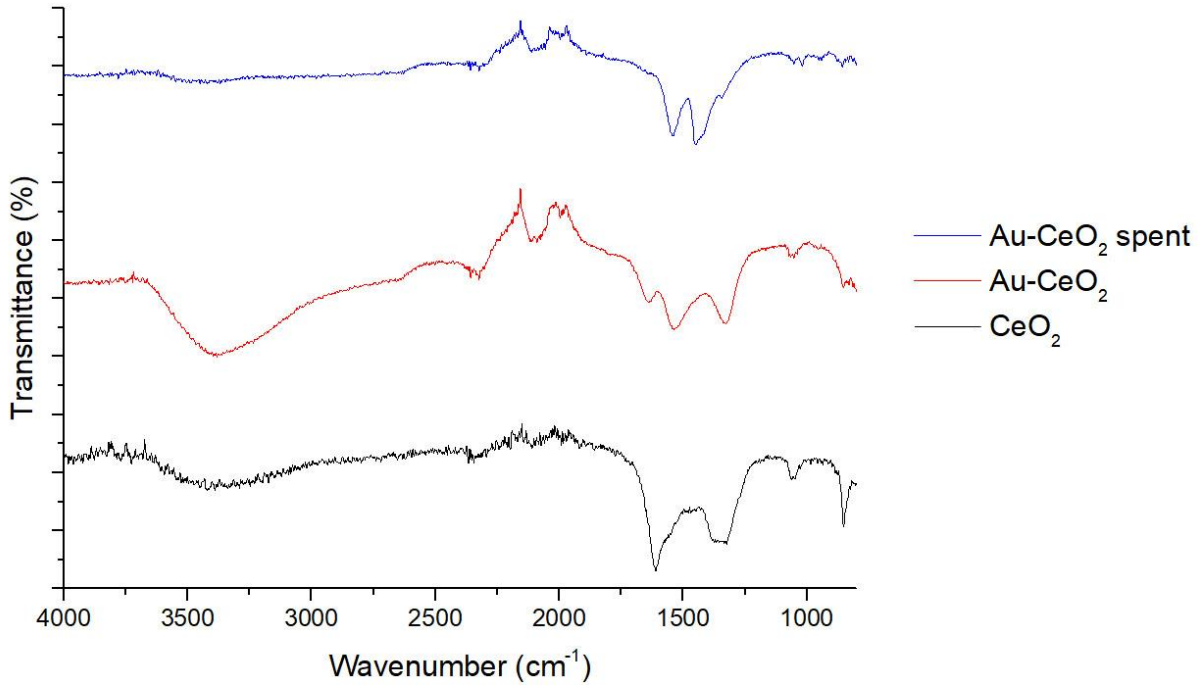

Figure 20. FT-IR spectra of CeO_2 (black), Au-CeO_2 (red) and Au-CeO_2 after EtOH oxidation at 150 °C for 4h (blue).

3.4 Chemical ligand removal from Au_9-SiO_2

Au_9 clusters are deposited on SiO_2 to obtain 0.5 wt% Au (called Au_9-SiO_2) and subsequently treated with a BCl_3 solution in DCM (called Au_9-SiO_2-treated). Their UV-Vis spectra and XRD diffractogram are shown in Figure 21. Au_9-SiO_2 shows clear absorbances of Au_9 clusters without distinguishable LSPR bands. After treatment with BCl_3, a white powder was obtained without the clear Au_9 cluster absorbance and LSPR bands. This indicates that the protective PPh_3 ligands might indeed be successfully removed from the Au core without causing sintering. Figure 21b shows an extra signal around 2θ = 32.5 ° after treatment indicating the formation of $B(OH)_3$, sassolite. This signal disappears after washing with water, but also resulted in Au sintering and leaching (Figure S12).

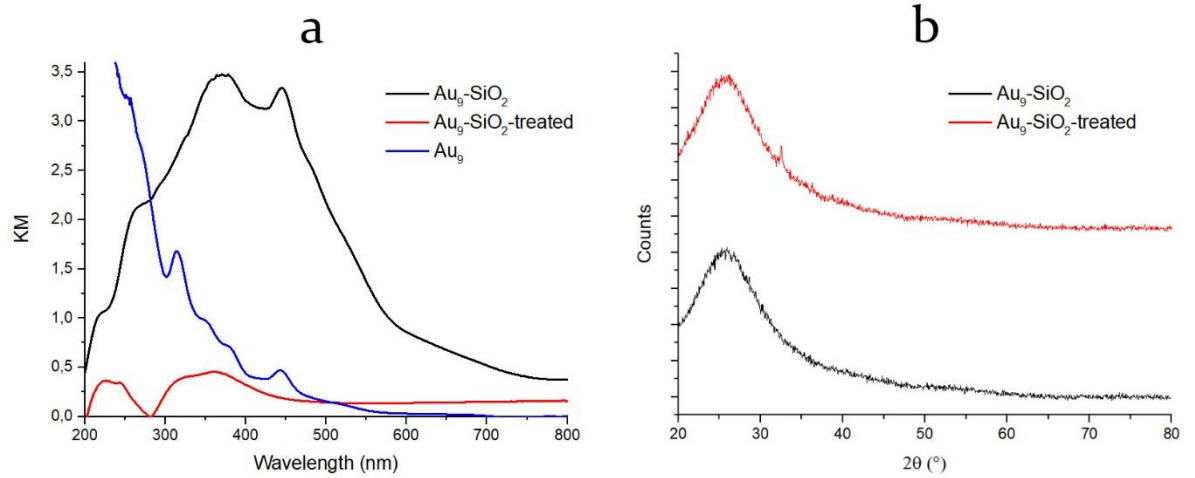

Figure 21. UV-Vis spectra (a) of Au_9-SiO_2 (black), Au_9-SiO_2-treated (red) and Au_9 clusters in EtOH (blue) and XRD diffractogram (b) of Au_9-SiO_2 (black) and Au_9-SiO_2-treated (red). Note that the UV-Vis spectrum of Au_9 clusters is measured dissolved in ethanol and does not possess the same y-axis but is still added for clarity.

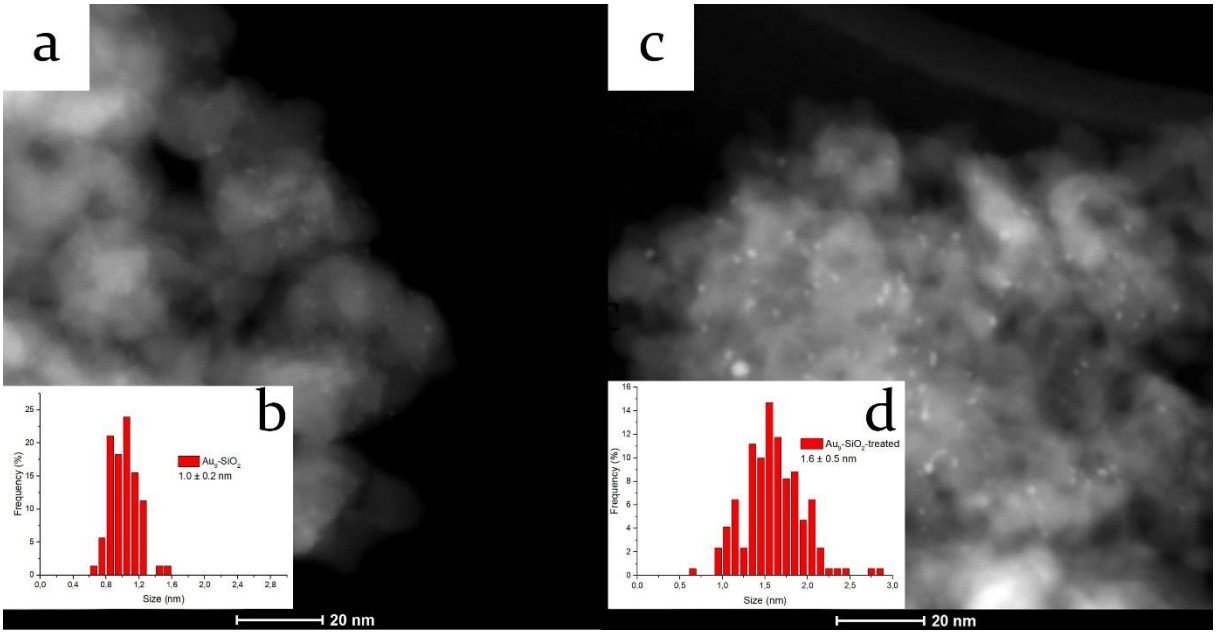

Figure 22. Typical TEM images and corresponding particle size distributions of Au_9-SiO_2 (a,b) and Au_9-SiO_2-treated (c,d).

Figure 22 shows TEM images and particle size distributions of Au_9-SiO_2 before and after BCl_3 treatment. Initially, their Au particle size is around 1.0 nm, which is in accordance to literature known about Au_9 cluster.[88,89] After treatment, the particle size has increased to around 1.6 nm. This is too small for a LSPR effect to originate, which explains why it was not seen in UV-Vis. So even though the particles grow during the BCl_3 treatment, this sintering is limited to a certain extent as the cluster sizes are still fairly small.

Table 4. ICP results of Au-SiO_2 before and after BCl_3 treatment

Sample	Au (wt%)	P (wt%)	B (wt%)
Au-SiO_2	0.49	0.040	-
Au-SiO_2-treated	0.07	0.009	1.00

Table 4 shows the ICP results before and after BCl_3 treatment. It is clear that Au leaches from the SiO_2 surface after BCl_3 treatment and the ligand content (P) decreases. Note that not all PPh_3 is removed and some might still be present on the clusters surface. ICP also confirms the formation of $B(OH)_3$ left after BCl_3 treatment. The increase in particle size and leaching of Au make the BCl_3 treatment an unsuitable method for the investigation of Au cluster size on their catalytic activity.

4. Conclusion

CeO_2 rods, cubes and polyhedra can be synthesised with high purity using hydrothermal treatment. These materials exhibit ({110} and {111}), {100} and ({100} and {111}) exposed surface planes, respectively. The rods and cubes were best at stabilizing Au_9 clusters compared to polyhedra. Even though CeO_2 is an active support, Au increases its selectivity and activity towards acetaldehyde in ethanol oxidation. Au_n nanoparticles are more active compared to all used clusters, but their higher selectivity towards CO_2 may have resulted in binding of polydentate carbonates to the active sites on CeO_2 which deactivated the catalyst. Furthermore, a decrease of cluster size by only one atom (Au_9 → Au_8) resulted in a decrease in oxidation activity, while a bimetallic cluster (Au_6Pd) did not show a much higher activity contrary to previous beliefs for bimetallic particles. Next to this, treatment of Au_9 clusters deposited on SiO_2 with BCl_3 resulted removal of protective PPh_3 ligands, growth of the Au nanoparticle size and Au leaching which makes the treatment unsuitable for the investigation of Au cluster size and composition effects in heterogeneous catalysis.

5. Outlook

To further understand the stabilizing properties of the different CeO_2 surface planes towards Au sintering, H_2-TPR could be measured. Each CeO_2 sample should first be dried and subsequently heated to high temperatures under O_2 flow as a pre-treatment to make sure all surfaces are fully oxidised. Hereafter, their H_2 consumption and reducibility can be measured which might explain their differences in stabilising properties.

It is not exactly known whether the cluster sizes are kept intact during catalysis or whether the TOFs calculated are actually corresponding the activities of ligands-less clusters, especially in the case for Au_6Pd . To test this, all clusters should first be pre-treated at 120 °C for 4h in air and check for sintering (using TEM or EXAFS) before catalysis. Another model reaction could also be used that is less likely to enhance nanoparticle sintering to ensure the cluster sizes are kept intact. Also, metal loadings should be determined using ICP in order to calculate more precise TOF values.

The Au nanoparticles are more active compared to Au clusters because of their possible stronger interaction with the support after calcination at 400 °C. To test this, deposited (Au_9) clusters should also be calcined at 400 °C before catalysis. This might result in a higher activity of Au_9 clusters, even though the particles will probably grow to larger sizes.

To confirm whether the NO_3^- anions actually do have a negative effect on the activity of Au clusters, the catalysts should first be reduced before catalysis under H_2. If this is the case, a higher activity could be expected, but the cluster atomicity will probably also change upon reduction.

Other experiments could be done using another lighter Lewis acidic support than CeO_2, like γ-Al_2O_3 or TiO_2. These supports could also activate the clusters by removing the ligands from the Au core while providing a better contrast in TEM for particle size determination.

6. Acknowledgements

Firstly, I want to thank Baira Donoeva for daily supervision and making it possible for me to do my master thesis at ICC. She was always open for questions and discussion while giving good advice on interesting experiments to do.

I also want to thank Jongkook Hwank, Johan de Boed and Petra Keijzer for assistance on the lab and supervision using the oxidation setup.

Finally, I want to thank all other master students at ICC for fruitful discussions which were honestly not always about the subject of this thesis.

7. References

1. Haruta, M., Yamada, N., Kobayashi, T. & Iijima, S. Gold catalysts prepared by coprecipitation for low-temperature oxidation of hydrogen and of carbon monoxide. *J. Catal.* **115**, 301–309 (1989).

2. Tantayanon, S. & Kiatisevi, S. The chemical society of Thailand. *Chem. - An Asian J.* **6**, 2184–2186 (2011).

3. Haruta, M. Size- and support-dependency in the catalysis of gold. *Catal. Today* **36**, 153–166 (1997).

4. Hughes, M. D. *et al.* Tunable gold catalysts for selective hydrocarbon oxidation under mild conditions. *Nature* **437**, 1132–1135 (2005).

5. Huang, J. *et al.* Propene epoxidation with dioxygen catalyzed by gold clusters. *Angew. Chemie - Int. Ed.* **48**, 7862–7866 (2009).

6. Turner, M. *et al.* Selective oxidation with dioxygen by gold nanoparticle catalysts derived from 55-atom clusters. *Nature* **454**, 981–983 (2008).

7. Castleman, A. W. & Bowen, K. H. Clusters: Structure, energetics, and dynamics of intermediate states of matter. *J. Phys. Chem.* **100**, 12911–12944 (1996).

8. *Nanocatalysis*. (Springer, Berlin, Heidelberg, 2007).

9. Edwards, P. P. & Thomas, J. M. Gold in a metallic divided state - From Faraday to present-day nanoscience. *Angew. Chemie - Int. Ed.* **46**, 5480–5486 (2007).

10. Jiang, T. *et al.* Trends in CO oxidation rates for metal nanoparticles and close-packed, stepped, and kinked surfaces. *J. Phys. Chem. C* **113**, 10548–10553 (2009).

11. Tsunoyama, H. *et al.* Size-Controlled Synthesis of Gold Clusters as Efficient Catalysts for Aerobic Oxidation. *Catal. Surv. from Asia* **15**, 230–239 (2011).

12. Chen, Y., Li, G., Qian, H. & Jin, R. Catalysis by Atomically Precise Gold Nanoclusters. *Catal. by Mater. with Well-Defined Struct.* 239–262 (2015). doi:10.1016/B978-0-12-801217-8.00008-6

13. Yoon, B., Ha, H. & Landman, U. interaction of O2 with gold clusters.pdf. 4066–4071 (2003).

14. Salisbury, B. E., Wallace, W. T. & Whetten, R. L. Low-temperature activation of molecular oxygen by gold clusters: A stoichiometric process correlated to electron affinity. *Chem. Phys.* **262**, 131–141 (2000).

15. Hansen, K. Thermal damping of odd-even effects in gold clusters. *Chem. Phys.* **530**, 110637 (2020).

16. Nijamudheen, A. & Datta, A. Odd-even oscillations in structural and optical properties of gold clusters. *J. Mol. Struct. THEOCHEM* **945**, 93–96 (2010).

17. Huang, J. & Haruta, M. Heterogeneous Catalysis by Gold Clusters. in *Bridging Heterogeneous and Homogeneous Catalysis: Concepts, Strategies, and Applications* **9783527335**, 397–424 (2014).

18. Yamazoe, S., Koyasu, K. & Tsukuda, T. Nonscalable oxidation catalysis of gold clusters. *Acc. Chem. Res.* **47**, 816–824 (2014).

19. Liu, Y., Tsunoyama, H., Akita, T., Xie, S. & Tsukuda, T. Aerobic oxidation of cyclohexane catalyzed by size-controlled au clusters on hydroxyapatite: Size effect in the sub-2 nm regime. *ACS Catal.* **1**, 2–6 (2011).

20. Jin, R. Atomically precise metal nanoclusters: Stable sizes and optical properties. *Nanoscale* **7**, 1549–1565 (2015).

21. Choudhary, T. V. *et al.* CO oxidation on supported nano-Au catalysts synthesized from a [Au6(PPh3)6](BF4)2complex. *J. Catal.* **207**, 247–255 (2002).

22. Wan, X.-K., Wang, J.-Q., Nan, Z.-A. & Wang, Q.-M. Ligand Effects in Catalysis by Atomically

Precise Gold Clusters. *Sci. Adv.* **3**, e1701823 (2017).

23. Fang, J. *et al.* Recent advances in the synthesis and catalytic applications of ligand-protected, atomically precise metal nanoclusters. *Coord. Chem. Rev.* **322**, 1–29 (2016).

24. Thayer, A. M. Changing industry. *Nature* **183**, 655–657 (1959).

25. Ouds, G. & Macdonald, K. Gold Rush. *Probat. J.* **34**, 40 (1987).

26. Prati, L. & Rossi, M. Gold on carbon as a new catalyst for selective liquid phase oxidation of diols. *J. Catal.* **176**, 552–560 (1998).

27. Li, G. & Jin, R. Atomically precise gold nanoclusters as new model catalysts. *Acc. Chem. Res.* **46**, 1749–1758 (2013).

28. Adnan, R. H. & Golovko, V. B. Benzyl Alcohol Oxidation Using Gold Catalysts Derived from Au 8 Clusters on TiO 2. *Catal. Letters* **149**, 449–455 (2019).

29. Tsunoyama, H., Sakurai, H. & Tsukuda, T. Size effect on the catalysis of gold clusters dispersed in water for aerobic oxidation of alcohol. *Chem. Phys. Lett.* **429**, 528–532 (2006).

30. Tsunoyama, H., Sakurai, H., Negishi, Y. & Tsukuda, T. Size-specific catalytic activity of polymer-stabilized gold nanoclusters for aerobic alcohol oxidation in water. *J. Am. Chem. Soc.* **127**, 9374–9375 (2005).

31. Navas, J. *et al.* Exceptional oxidation activity with size-controlled supported gold clusters of low atomicity. *Nat. Chem.* **5**, 775–781 (2013).

32. Vajda, S. *et al.* Supported gold clusters and cluster-based nanomaterials: characterisation, stability and growth studies by in situ GISAXS under vacuum conditions and in the presence of hydrogen. *Top. Catal.* **39**, 161–166 (2006).

33. Min, B. K., Santra, A. K. & Goodman, D. W. Understanding silica-supported metal catalysts: Pd/silica as a case study. *Catal. Today* **85**, 113–124 (2003).

34. Déronzier, T., Morfin, F., Lomello, M. & Rousset, J. L. Catalysis on nanoporous gold-silver systems: Synergistic effects toward oxidation reactions and influence of the surface composition. *J. Catal.* **311**, 221–229 (2014).

35. Bracey, C. L., Ellis, P. R. & Hutchings, G. J. Application of copper-gold alloys in catalysis: Current status and future perspectives. *Chem. Soc. Rev.* **38**, 2231–2243 (2009).

36. Xie, S., Tsunoyama, H., Kurashige, W., Negishi, Y. & Tsukuda, T. Enhancement in aerobic alcohol oxidation catalysis of Au25clusters by single Pd atom doping. *ACS Catal.* **2**, 1519–1523 (2012).

37. Liu, P. & Nørskov, J. K. Ligand and ensemble effects in adsorption on alloy surfaces. *Phys. Chem. Chem. Phys.* **3**, 3814–3818 (2001).

38. Jirkovský, J. S. *et al.* Single atom hot-spots at Au-Pd nanoalloys for electrocatalytic H2O2production. *J. Am. Chem. Soc.* **133**, 19432–19441 (2011).

39. Hemmingson, S. L., James, T. E., Feeley, G. M., Tilson, A. M. & Campbell, C. T. Adsorption and Adhesion of Au on Reduced CeO2(111) Surfaces at 300 and 100 K. *J. Phys. Chem. C* **120**, 12113–12124 (2016).

40. Farmer, J. A. & Campbell, C. T. Ceria maintains smaller metal catalyst particles by strong metal-support bonding. *Science (80-.).* **329**, 933–936 (2010).

41. Hu, S. *et al.* Ag nanoparticles on reducible CeO2(111) thin films: Effect of thickness and stoichiometry of ceria. *J. Phys. Chem. C* **119**, 3579–3588 (2015).

42. Rodriguez, J. A., Grinter, D. C., Liu, Z., Palomino, R. M. & Senanayake, S. D. Ceria-based model catalysts: Fundamental studies on the importance of the metal-ceria interface in CO oxidation, the water-gas shift, CO2 hydrogenation, and methane and alcohol reforming. *Chem. Soc. Rev.* **46**, 1824–1841 (2017).

43. Kašpar, J., Fornasiero, P. & Graziani, M. Use of CeO2-based oxides in the three-way catalysis. *Catal. Today* **50**, 285–298 (1999).

44. Si, R., Zhang, Y. W., Li, S. J., Lin, B. X. & Yan, C. H. Urea-based hydrothermally derived homogeneous nanostructured Ce 1-xZrxO2 (x = 0-0.8) solid solutions: A strong correlation between oxygen storage capacity and lattice strain. *J. Phys. Chem. B* **108**, 12481–12488 (2004).

45. Trovaelly, A. *Catalysis by Ceria and Related Materials, ed. A. Trovarelli and P. Fornasiero, Imperial College Press, London (UK), 2013.* (Imperial College Press, 2002).

46. Cormack, A. N., Lamphier, S., Wang, B., Gubb, T. & Reed, K. Simulations of ceria nanoparticles. *Proc. R. Soc. A Math. Phys. Eng. Sci.* **471**, 1–11 (2015).

47. Tuller, H. L. Ionic conduction in nanocrystalline materials. **131**, 143–157 (2014).

48. Burch, R. Gold catalysts for pure hydrogen production in the water-gas shift reaction: Activity, structure and reaction mechanism. *Phys. Chem. Chem. Phys.* **8**, 5483–5500 (2006).

49. Jun, Y. W., Choi, J. S. & Cheon, J. Shape control of semiconductor and metal oxide nanocrystals through nonhydrolytic colloidal routes. *Angew. Chemie - Int. Ed.* **45**, 3414–3439 (2006).

50. Castellarin-Cudia, C. *et al.* Strain-induced formation of arrays of catalytically active sites at the metal-oxide interface. *Surf. Sci.* **554**, (2004).

51. Berner, U. *et al.* Ultrathin ordered CeO overlayers on Pt (111): interaction with NO , NO , H O and CO. *Surf. Sci.* **467**, 201–213 (2000).

52. Abad, A., Concepción, P., Corma, A. & García, H. A collaborative effect between gold and a support induces the selective oxidation of alcohols. *Angew. Chemie - Int. Ed.* **44**, 4066–4069 (2005).

53. Chojnack, T., Krause, K., Schmidt, L. D. & Cbt, G. Microstructure and Reactivity of Pt-Ce and R h - C e Particles on Silica 1 Pt and Rh catalyst particles are uniquely capable of the simultaneous oxidation of CO and hydrocarbons and the reduction of NO to promote the water-gas shift reaction , to environm. *J. Catal.* **138**, 283–93 (1991).

54. Kundakovic, L. & Flytzani-Stephanopoulos, M. Cu- and Ag-modified cerium oxide catalysts for methane oxidation. *J. Catal.* **179**, 203–221 (1998).

55. Si, R. & Flytzani-Stephanopoulos, M. Shape and crystal-plane effects of nanoscale ceria on the activity of Au-CeO2 catalysts for the water-gas shift reaction. *Angew. Chemie - Int. Ed.* **47**, 2884–2887 (2008).

56. Sayle, T. X. T., Parker, S. C. & Sayle, D. C. Oxidising CO to CO2using ceria nanoparticles. *Phys. Chem. Chem. Phys.* **7**, 2936–2941 (2005).

57. Mai, H. X. *et al.* Shape-selective synthesis and oxygen storage behavior of ceria nanopolyhedra, nanorods, and nanocubes. *J. Phys. Chem. B* **109**, 24380–24385 (2005).

58. Mullins, D. R. The Surface Chemistry of Cerium Oxide. *J. Chem. Inf. Model.* **53**, 1689–1699 (2013).

59. Skoog, D. A., Holler, F. J. & Crouch, S. R. *Principles of Instrumental Analysis*. (Thomson Brooks/Cole, 2007).

60. Higaki, T. *et al.* Sharp Transition from Nonmetallic Au246 to Metallic Au279 with Nascent Surface Plasmon Resonance. *J. Am. Chem. Soc.* **140**, 5691–5695 (2018).

61. Kamat, P. V. Photophysical, photochemical and photocatalytic aspects of metal nanoparticles. *J. Phys. Chem. B* **106**, 7729–7744 (2002).

62. Zhou, M., Zeng, C., Li, Q., Higaki, T. & Jin, R. Gold Nanoclusters: Bridging Gold Complexes and Plasmonic Nanoparticles in Photophysical Properties. *Nanomaterials* **9**, 933 (2019).

63. Rothenberg, G. *Catalysis*. (Wiley-VCH, 2008).

64. Geelen, D. *et al.* eV-TEM: Transmission electron microscopy in a low energy cathode lens

instrument. *Ultramicroscopy* **159**, 482–487 (2015).

65. Malatesta, L., Naldini, L., Simonetta, G. & Cariati, F. Triphenylphosphine-gold(0) gold(I) compounds. *Chem. Commun.* **1**, 212–213 (1965).

66. Malvano, M. L. No Title. *Atti della R. Accad. dei Lincei* **17**, 151 (1908).

67. Wen, F., Englert, U., Gutrath, B. & Simon, U. Crystal structure, electrochemical and optical properties of [Au 9(PPh3)8](NO3)3. *Eur. J. Inorg. Chem.* **9**, 106–111 (2008).

68. van der Yelden, J. W. A., Bour, J. J., Bosman, W. P. & Noordik, J. H. Reactions of Cationic Gold Clusters with Lewis Bases. Preparation and X-ray Structure Investigation of [Au8(PPh3)7](NO3)2·2CH2Cl2 and Au6(PPh3)4[Co(CO)4]2. *Inorg. Chem.* **22**, 1913–1918 (1983).

69. Matsuo, S., Takano, S., Yamazoe, S., Koyasu, K. & Tsukuda, T. Selective and High-Yield Synthesis of Oblate Superatom $[PdAu_8(PPh_3)_8]^{2+}$. *ChemElectroChem* **3**, 1206–1211 (2016).

70. Quintilio, W., Sotelo, A. & Felicissimo, A. M. P. A New Synthesis, Properties and Spectroscopic Characterisation of [(PPh3)Pd(AuPPh3)6](N03)2. *Spectrosc. Lett.* **27**, 605–611 (1994).

71. Rodriguez, J. A. *et al.* Active gold-ceria and gold-ceria/titania catalysts for CO oxidation: From single-crystal model catalysts to powder catalysts. *Catal. Today* **240**, 229–235 (2015).

72. Yang, Y. *et al.* Redox enzyme-mimicking activities of CeO2 nanostructures: Intrinsic influence of exposed facets. *Sci. Rep.* **6**, 1–7 (2016).

73. Sujana, M. G., Chattopadyay, K. K. & Anand, S. Characterisation and optical properties of nano-ceria synthesized by surfactant-mediated precipitation technique in mixed solvent system. *Appl. Surf. Sci.* **254**, 7405–7409 (2008).

74. Renuka, N. K. Structural characteristics of quantum-size ceria nano particles synthesized via simple ammonia precipitation. *J. Alloys Compd.* **513**, 230–235 (2012).

75. Tsunekawa, S., Fukuda, T. & Kasuya, A. Blue shift in ultraviolet absorption spectra of monodisperse CeO 2-x nanoparticles. *J. Appl. Phys.* **87**, 1318–1321 (2000).

76. Sakpal, T. & Lefferts, L. Structure-dependent activity of CeO2 supported Ru catalysts for CO2 methanation. *J. Catal.* **367**, 171–180 (2018).

77. Agarwal, S. *et al.* Exposed surfaces on shape-controlled ceria nanoparticles revealed through AC-TEM and water-gas shift reactivity. *ChemSusChem* **6**, 1898–1906 (2013).

78. Ma, Z. *et al.* Response mechanism of the docosahexaenoic acid producer Aurantiochytrium under cold stress. *Algal Res.* **25**, 191–199 (2017).

79. Longo, A., Boed, J. De, Linden, M. Van Der, Jongh, P. De & Donoeva, B. Atomically precise sub-nm supported Au clusters from phos- phine-stabilized precursors : the critical role of the support. (unpublished).

80. Sayle, T. X. T., Parker, S. C. & Catlow, C. R. A. The role of oxygen vacancies on ceria surfaces in the oxidation of carbon monoxide. *Surf. Sci.* **316**, 329–336 (1994).

81. Qiao, Z. A., Wu, Z. & Dai, S. Shape-controlled ceria-based nanostructures for catalysis applications. *ChemSusChem* **6**, 1821–1833 (2013).

82. Rodriguez, J. A., Liu, P., Hrbek, J., Evans, J. & Pérez, M. Water gas shift reaction on Cu and Au nanoparticles supported on CeO 2(111) and ZnO(0001): Intrinsic activity and importance of support interactions. *Angew. Chemie - Int. Ed.* **46**, 1329–1332 (2007).

83. Gamarra, D. & Martínez-Arias, A. Preferential oxidation of CO in rich H2 over CuO/CeO2: Operando-DRIFTS analysis of deactivating effect of CO2 and H2O. *J. Catal.* **263**, 189–195 (2009).

84. Yoon, B., Häkkinen, H. & Landman, U. Interaction of O 2 with gold clusters: Molecular and dissociative adsorption. *J. Phys. Chem. A* **107**, 4066–4071 (2003).

85. Yoshikawa, K., Sato, H., Kaneeda, M. & Kondo, J. N. Synthesis and analysis of CO2 adsorbents based on cerium oxide. *J. CO2 Util.* **8**, 34–38 (2014).

86. Vayssilov, G. N., Mihaylov, M., Petkov, P. S., Hadjiivanov, K. I. & Neyman, K. M. Reassignment of the vibrational spectra of carbonates, formates, and related surface species on ceria: A combined density functional and infrared spectroscopy investigation. *J. Phys. Chem. C* **115**, 23435–23454 (2011).

87. Li, T. J. Infrared Spectra and Characteristic Frequencies of Inorganic Ions. *Wuli Xuebao/Acta Phys. Sin.* **58**, 3665–3669 (2009).

88. Liu, Y., Tsunoyama, H., Akita, T. & Tsukuda, T. Preparation of ∼1 nm Gold Clusters Confined within Mesoporous Silica and Microwave-Assisted Catalytic Application for Alcohol Oxidation. *J. Phys. Chem. C* **113**, 13457–13461 (2009).

89. Wulansari, N., Mahawati, E. & Hartini, E. Gold Molecular Clusters to Nanoparticles : A Bottom-up Approach to Supported Nanoparticles for Heterogeneous Catalysis. (2013).

8. Supplementary information

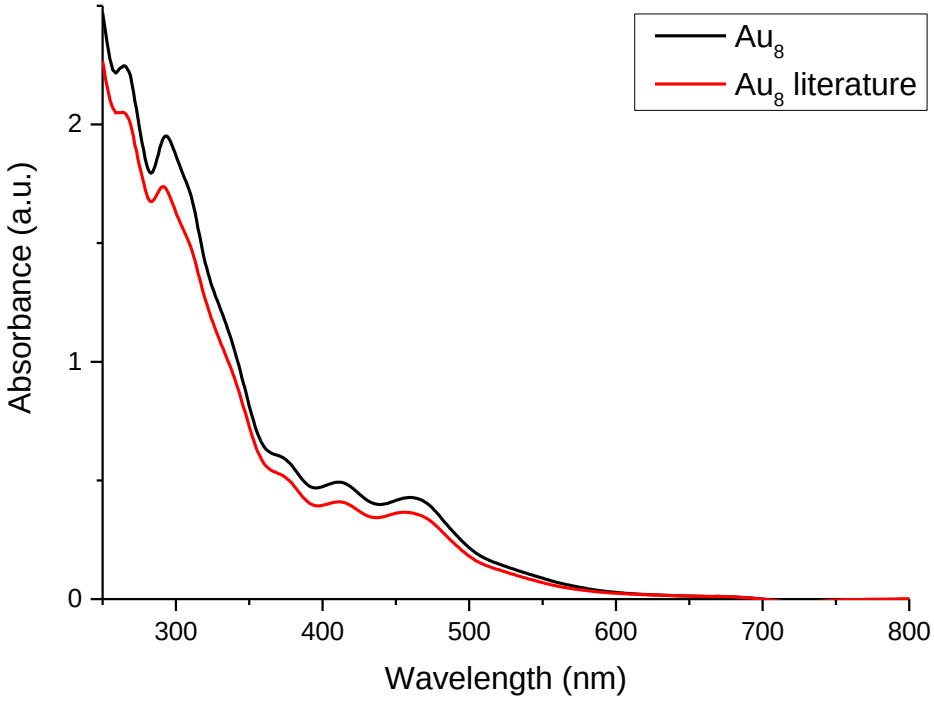

Figure S1. UV-Vis measured of the Au_8 clusters synthesised (black) and literature reference[79] (red) dissolved in EtOH.

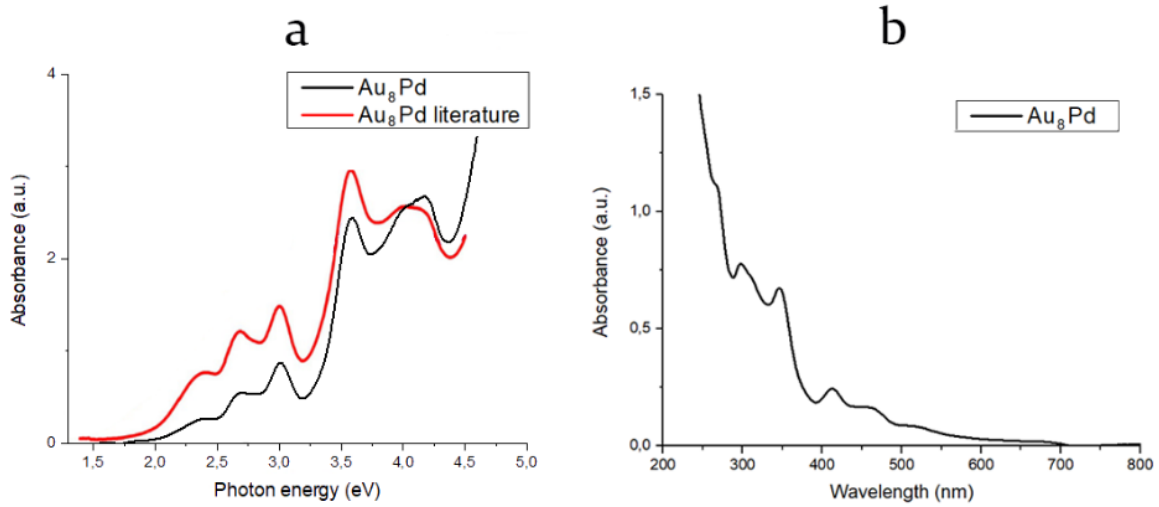

Figure S2. UV-Vis spectra of the synthesised $[Au_8Pd(PPh_3)_8]Cl_2$ cluster dissolved in EtOH with (a) and without (b) literature reference[69] for comparison. Note that the graphs have different x-axis.

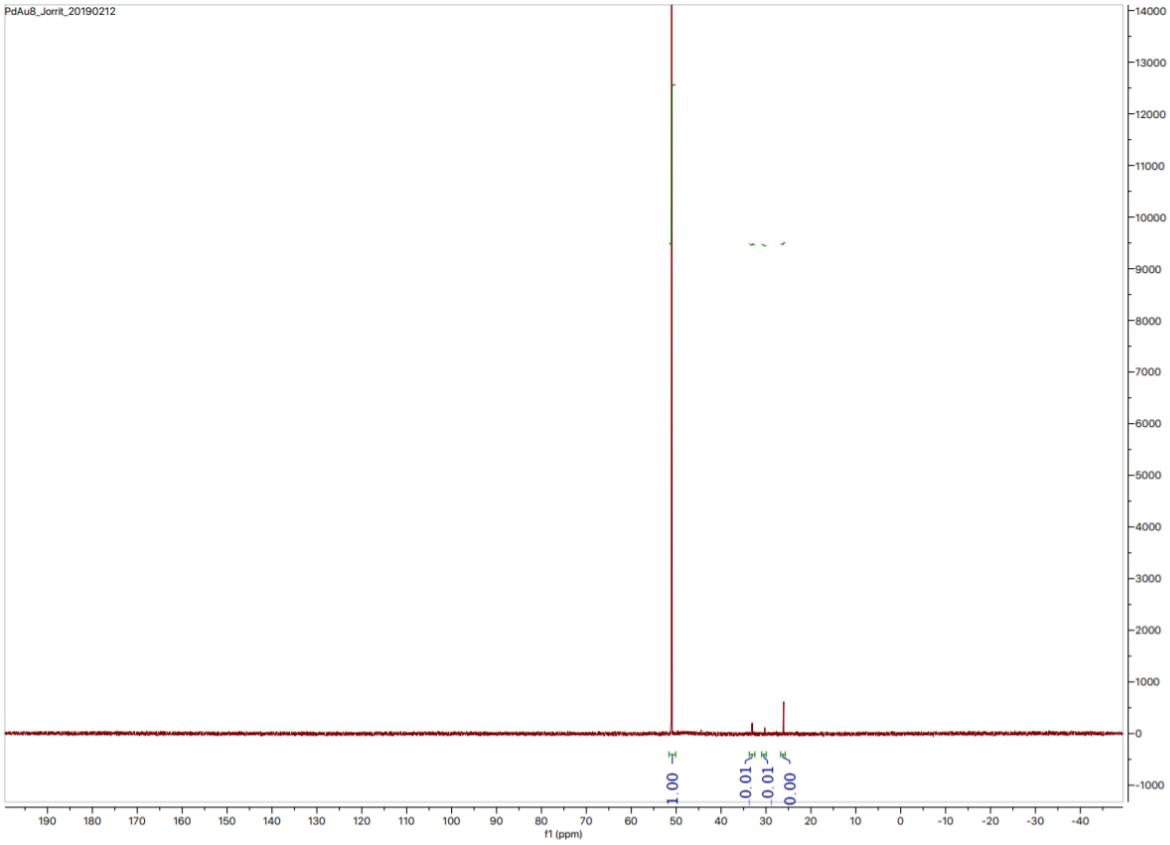

Figure S3. ^{31}P-NMR measured of the synthesised $[Au_8Pd(PPh_3)_8]Cl_2$ cluster dissolved in CD_3CN.

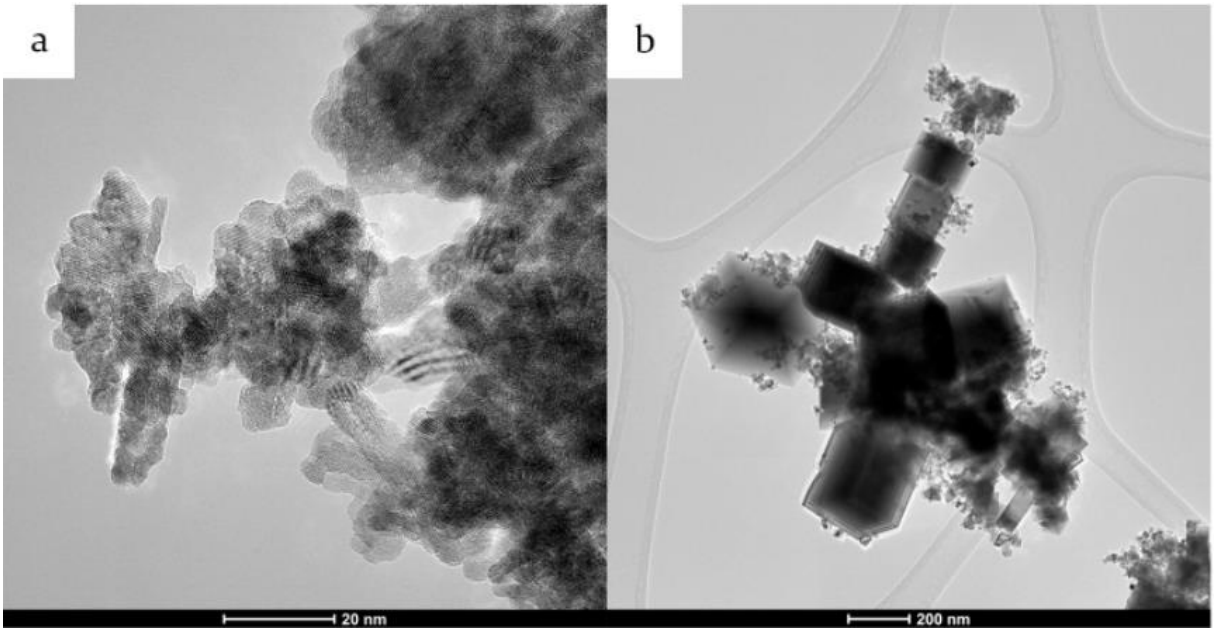

Figure S4. TEM images of CeO_2 'rods' (a) and CeO_2 cubes (b) synthesised without first dissolving the $Ce(NO)_3{\cdot}3H_2O$ separately in water.

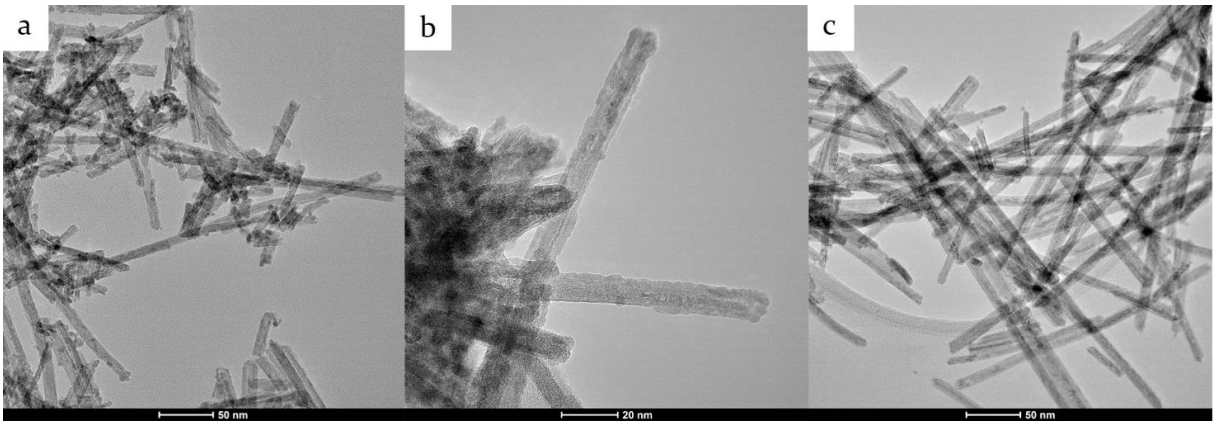

Figure S5. TEM images of CeO_2 synthesised with quickly quenching in water (a,b) and slowly cooling overnight in oven (c) after hydrothermal treatment.

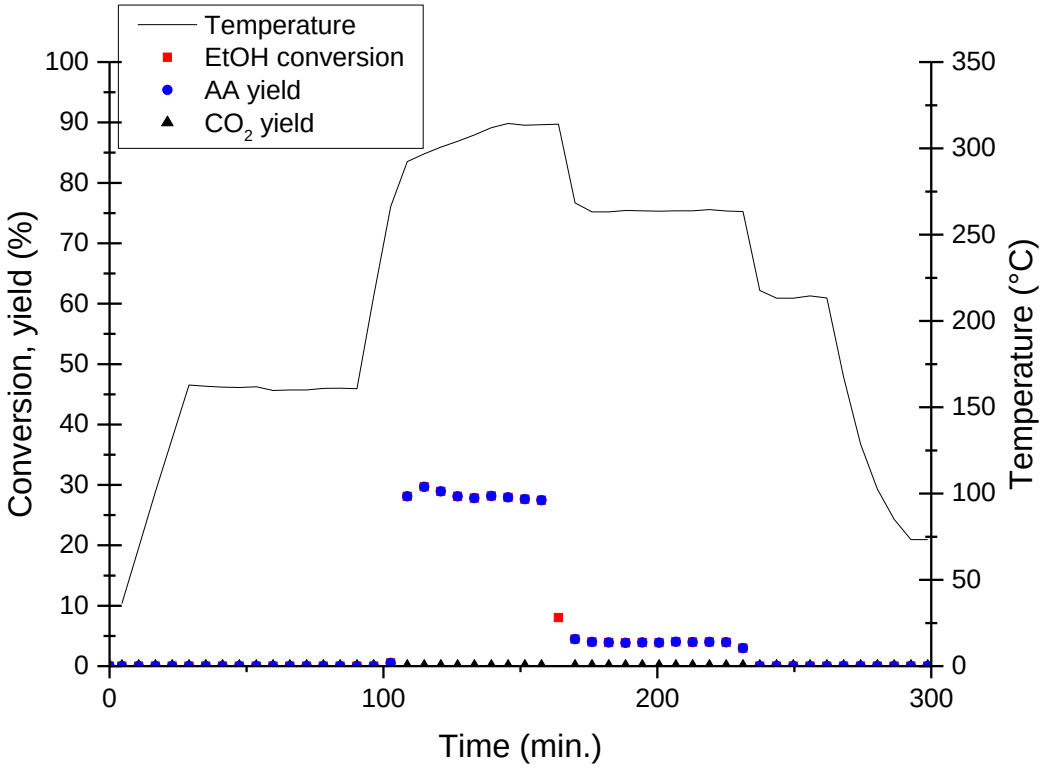

Figure S6. Ethanol oxidation without any catalyst.

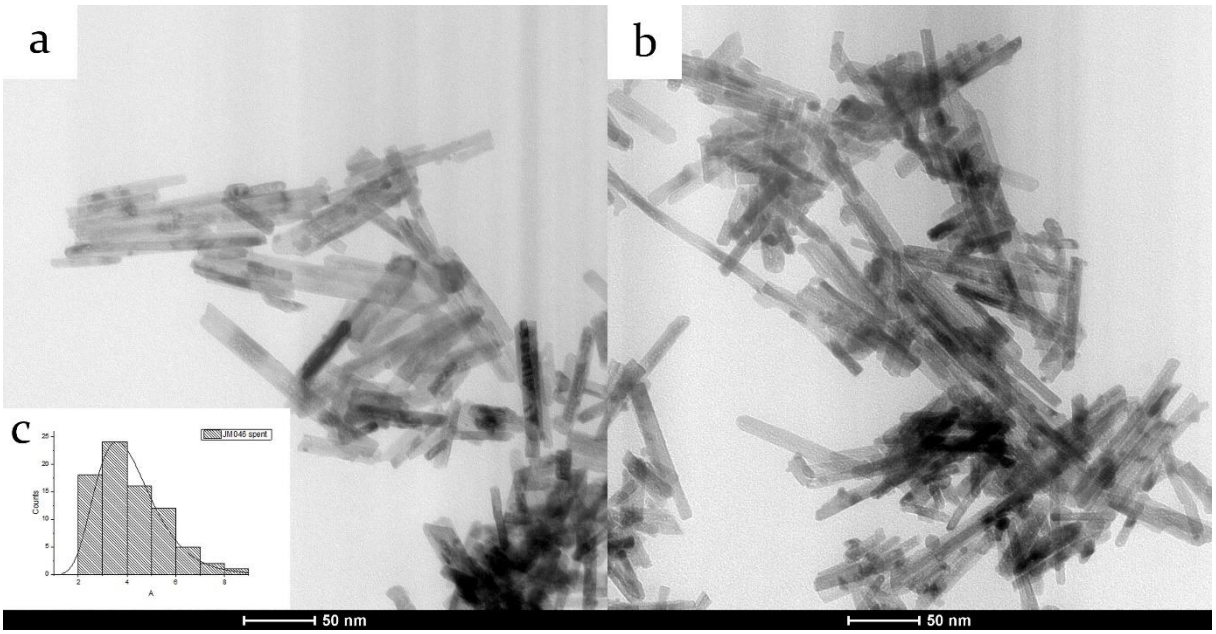

Figure S7. TEM images of spent 0.61 wt% Au_9-R catalyst (a,b) and their corresponding particle size distribution (c).

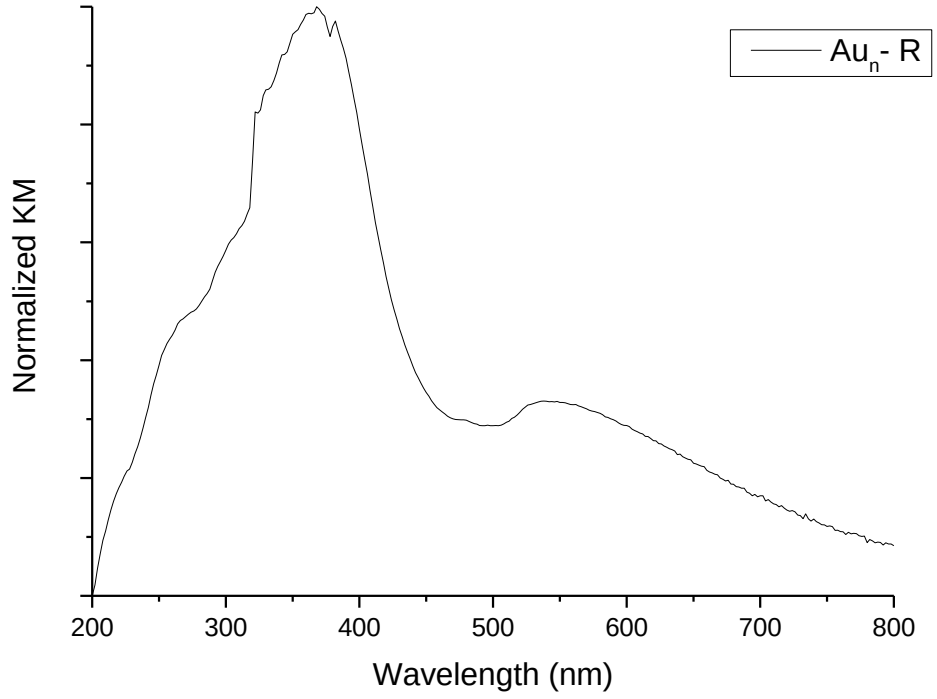

Figure S8. UV-Vis spectra of Au nanoparticles grown on CeO_2 rods.

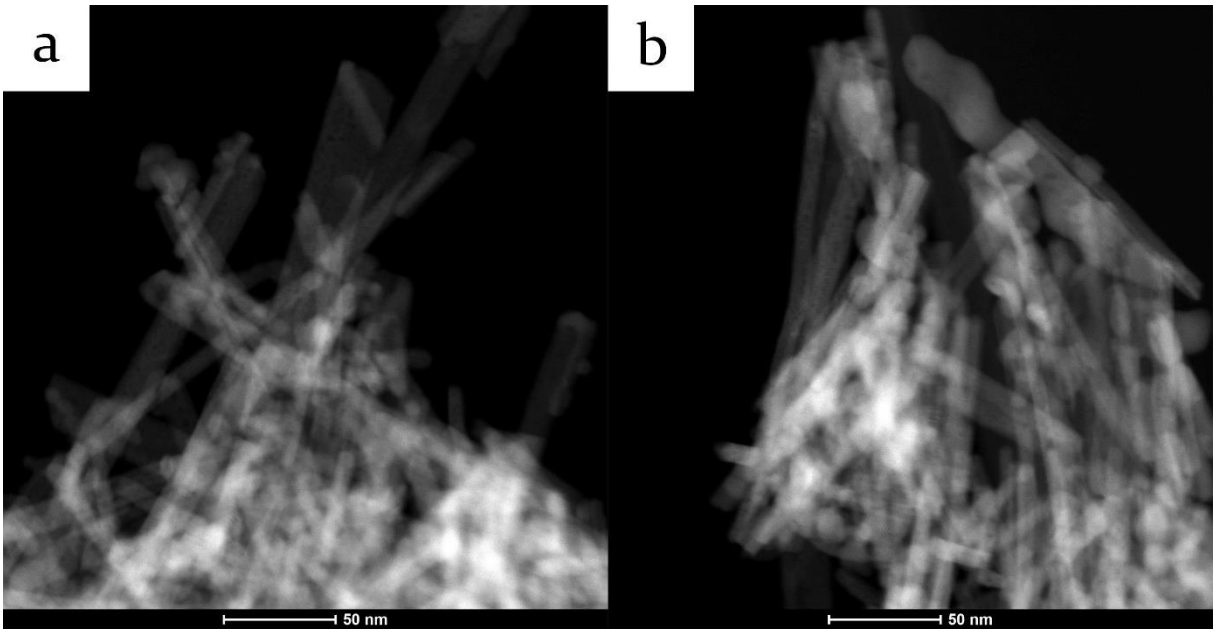

Figure S9. HAADF-STEM images of Au nanoparticles grown on CeO_2.

$$conversion_{ethanol}\ (mol\ h^{-1}) = \frac{flow_{ethanol}(L\ h^{-1}) * (converison_{cat}(\%) - conversion_{blank\ CeO2}) * 10^{-2} * P(bar)}{R(L \cdot bar \cdot K^{-1} \cdot mol^{-1}) * T_{GC}(K)} \qquad \text{Equation S1}$$

$$TOF\ (mol_{ethanol}\ mol^{-1}_{surface\ metal}\ h^{-1}) = \frac{converison_{ethanol}(mol\ h^{-1})}{mass_{metal}\ (g) * molar\ mass_{metal}(g\ mol^{-1})} \qquad \text{Equation S2}$$

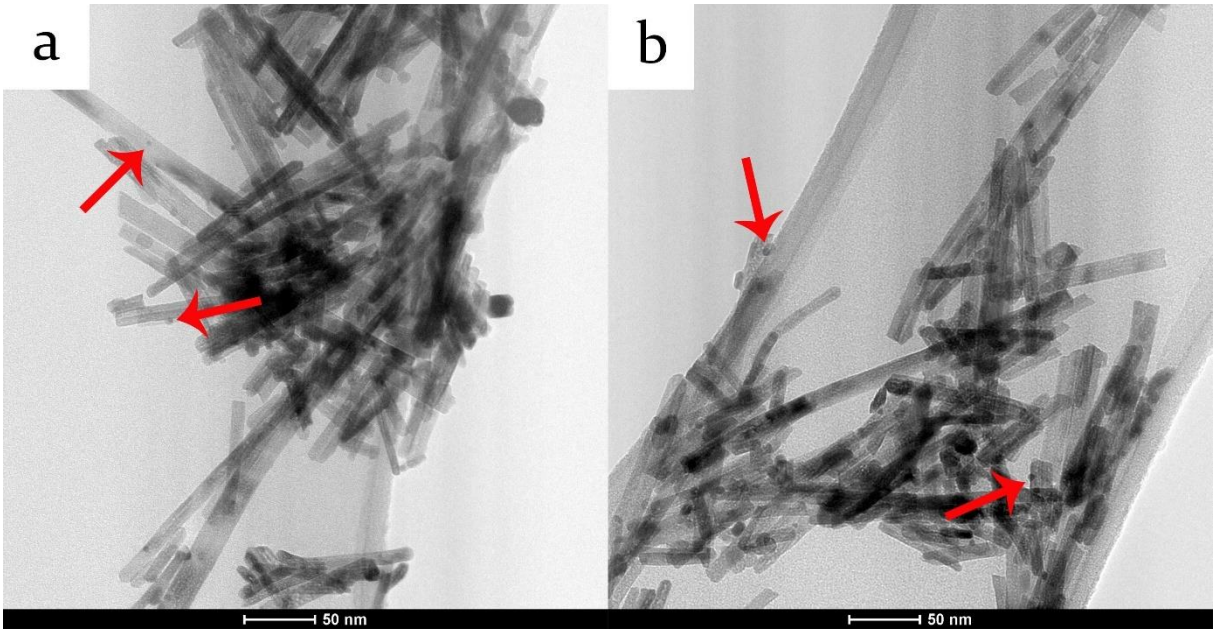

Figure S10. TEM images of Au_9-R after EtOH oxidation at 150 °C for 1.5h.

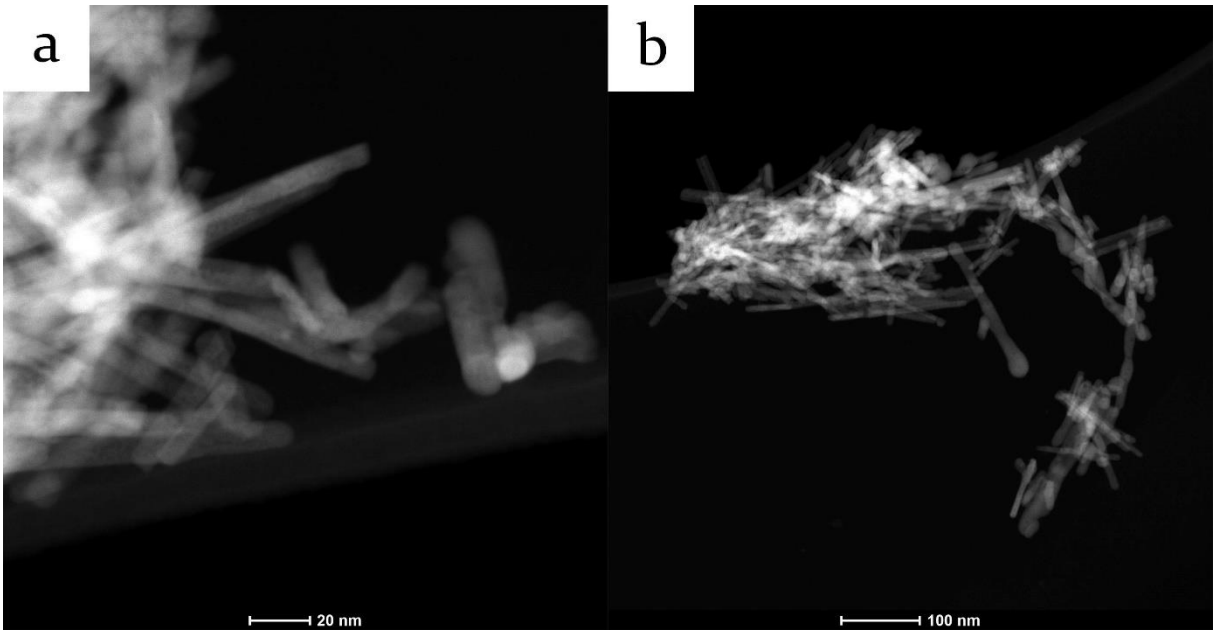

Figure S11. HAADF-STEM images of Au_n-CeO_2 after EtOH oxidation at 150 °C for 1.5h.

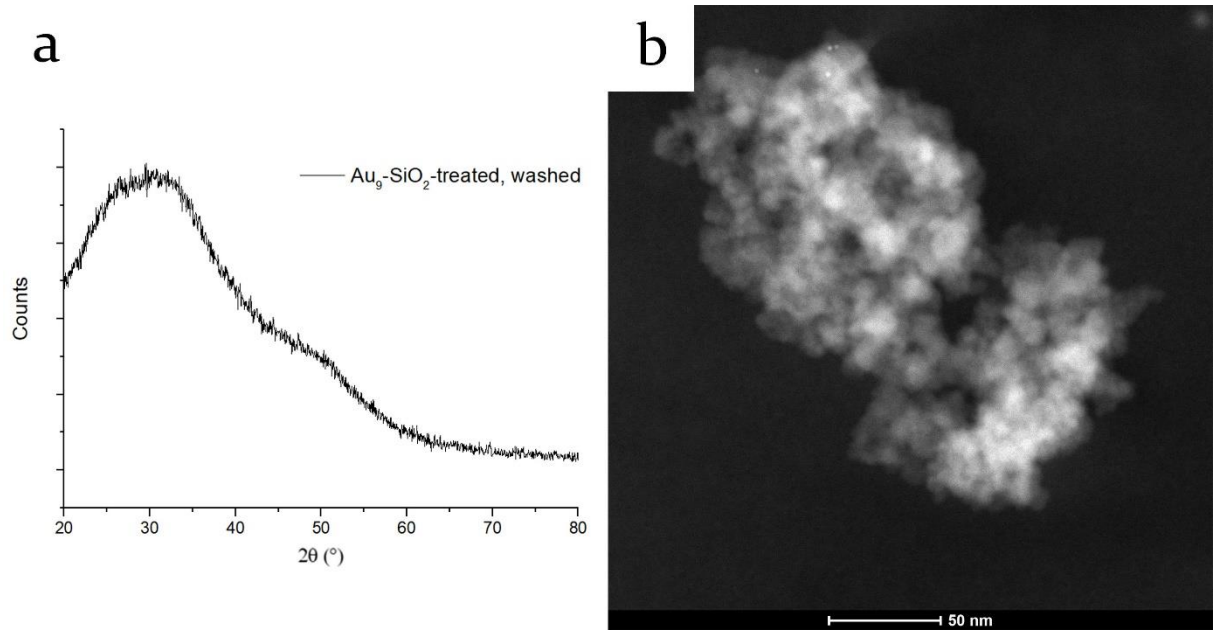

Figure S12. XRD diffractogram (a) and typical HAADF-STEM image (b) of Au_9-SiO_2-treated after washing with water.